University of Stavanger

Faculty of Science and Technology

MASTER'S THESIS

Study program/ Specialization: **MSc in Petroleum Engineering/Production**	Spring semester, 2012
Writer: **Remi-Erempagamo Meindinyo T.**	…… (Writer's signature)

Faculty supervisor: **Professor Rune W. Time (UiS)**

External supervisors: **Kristian Nordberg (Aker Solutions MMO)**

Henning Nordseth (Aker Solutions MMO)

Title of thesis:

Thermo-hydraulic Modeling of Flow in Flare Systems

Credits (ECTS): **30**

Key words: **Thermo-hydraulic parameters, Mach number, back-pressure, Flare system, Modeling, FlareNet, OLGA, Subsonic flow/Sonic flow**	Pages: 77 + enclosure: 86 Stavanger, June 2012

Table of Contents

Acknowldgement

I would love to thank members of the process department, Aker Solutions MMO, Stavanger; especially Study Manager Tore Berge, Specialist Engineer Kristian Nordberg, and Senior Engineer Henning Nordseth for sacrificing time and effort to support and accommodate me throughout this project. Providing me with the data and needed resources for this project.

I want to thank SPT Group for allowing me access to the use of OLGA version 7.1.1 for modeling during this project.

I want to thank my lecturers, Prof. Rune W. Time and Runar Boe, for the discussions we had, reviews and suggestions offered. That contributed to the success of this project.

Finally thanks to Jehovah God for giving me the grace and moral strength I needed through this project.

Abstract

Flare systems play a major role in the safety of Oil and Gas installations by serving as outlets for emergency pressure relief in case of process upsets. Accurate and reliable estimation of system thermo-hydraulic parameters, especially system back-pressure is critical to the integrity of a flare design.

FlareNet (Aspen Flare System Analyzer Version 7) is a steady state simulation tool tailored for flare system design and has found common use today. But design based on steady state modeling tends to be over conservative, due to the transient nature of the pressure relief processes in a flare system.

In this work an evaluation is done to see if OLGA (Version 7.1.1), a dynamic tool but not tailored for the high velocity flow common to flare systems, may be used for reliable dynamic modeling of a flare system. Simulations are run both in FlareNet and OLGA for a simple pipe system representing part of a flare network under steady state conditions. A comparison of the results from FlareNet and OLGA shows that OLGA estimates lie within acceptable ranges for subsonic flow. Observed differences in estimated back pressure are thoroughly analyzed, and reasons for such differences are stated. Recommendation is made that OLGA may be used for dynamic modeling of flare systems with reliable results that give a more realistic characterization of the processes taking place during pressure relief.

1. Introduction

1.1 General Background

Gas flaring is a common practice in the Oil and Gas industry during process upsets. As a major safety requirement at oil and gas installations such as refineries and process facilities, a flare system is usually installed to relieve built up pressure that may occur during shut down, start up or due to process system failure, reducing other safety hazards associated with process emergencies.

Accurate design of the flare system plays a key role in containing possible process safety hazards on the oil and gas installation, especially oil and gas offshore platforms. In order to enable uniformity and consistency, design guidelines and constraints are provided within the industry, both national and international standards – NORSOK, API and ISO – which serve as recommended practice in process and flare system design.

Thermo-hydraulic modeling serves a key role in flare system design. It enables the estimation of the thermodynamic and hydraulic parameters such as pressure, temperature, velocity/Mach, and other flow parameters required for building/modification of flare systems. There are several simulation tools used for flow simulation in the Oil and Gas industry. Some such as FlareNet, Flaresim, and g-Flare are specifically tailored for the modeling of flare systems. Others like HYSYS and OLGA have found wide use in process design and flow modeling, but are not particularly tailored for flare system design. FlareNet has found common use among many flare system design engineers, but it is only a steady-state tool; it only provides design results for a fixed time, with no full picture of the transient processes. OLGA and HYSYS on the other hand are both dynamic and steady state simulation tools, and would be very useful in characterizing the transient processes accompanying different process relief scenarios, i.e. during blow-down; a clear representation of how the flow-rate, pressure, temperature would change with time. Having a clear picture of these changes with time will contribute to more realistic and representative design.

Steady-state simulations have been run for a simple pipe system representing one part of a flare network. Simulation runs were done for different cases; a single component nitrogen gas flow, and multi-component hydrocarbon gas flow. Results have been compared for FlareNet and OLGA, and a difference in the back-pressure along the flare network was noticed for the two simulation tools, which increased in value with increasing flow-rate; reaching about 2 bar downstream the PSVs at a rate of 25MSm3/D for the multi-component hydrocarbon gas flow.

The main goal of this project is to investigate the implications of, and find out the reason for these differences. OLGA may be considered for transient modeling of flare systems if

1. The simulation tools worked within the confines of already established theory, with the significantly high flow rates encountered in flare systems,
2. The differences in back pressure can be explained.

1.2 Process Utility Systems

Offshore production systems starting from the Xmas tree basically consists of the gathering equipment, processing facility and flare system; connected by a network of pipes

Gathering equipment

The gathering equipment consisting of the production/injection manifold serves as a collection point for fluids from all the production wells or as a distribution unit for injection fluids to all injection wells via their respective Xmas trees.

Process facility

The process facility can mainly be referred to as the separation and compression equipment, fluid treatment equipment, with complementary equipment like boosters (pumps), heaters, coolers and heat exchangers.

Flare system

The flare system is the single largest pipe network on an offshore production platform. It serves as a relief system for depressurizing different process and production units in cases of shut down or unexpected cases of hazardous process emergencies, by collecting excess fluid through relief devices and a pipe network and disposing of it to the required outlet. The light hydrocarbons and other gases are released by combustion into the atmosphere while the heavier hydrocarbon, liquids are let out through drains and are often pumped back into the separation system.

Below is a descriptive figure showing a typical process utility systems network. The manifolds and process facilities can be critical channels for over pressure. They are thus usually tied to the flare via pressure relieving devices, to protect the system in case of pressure build up.

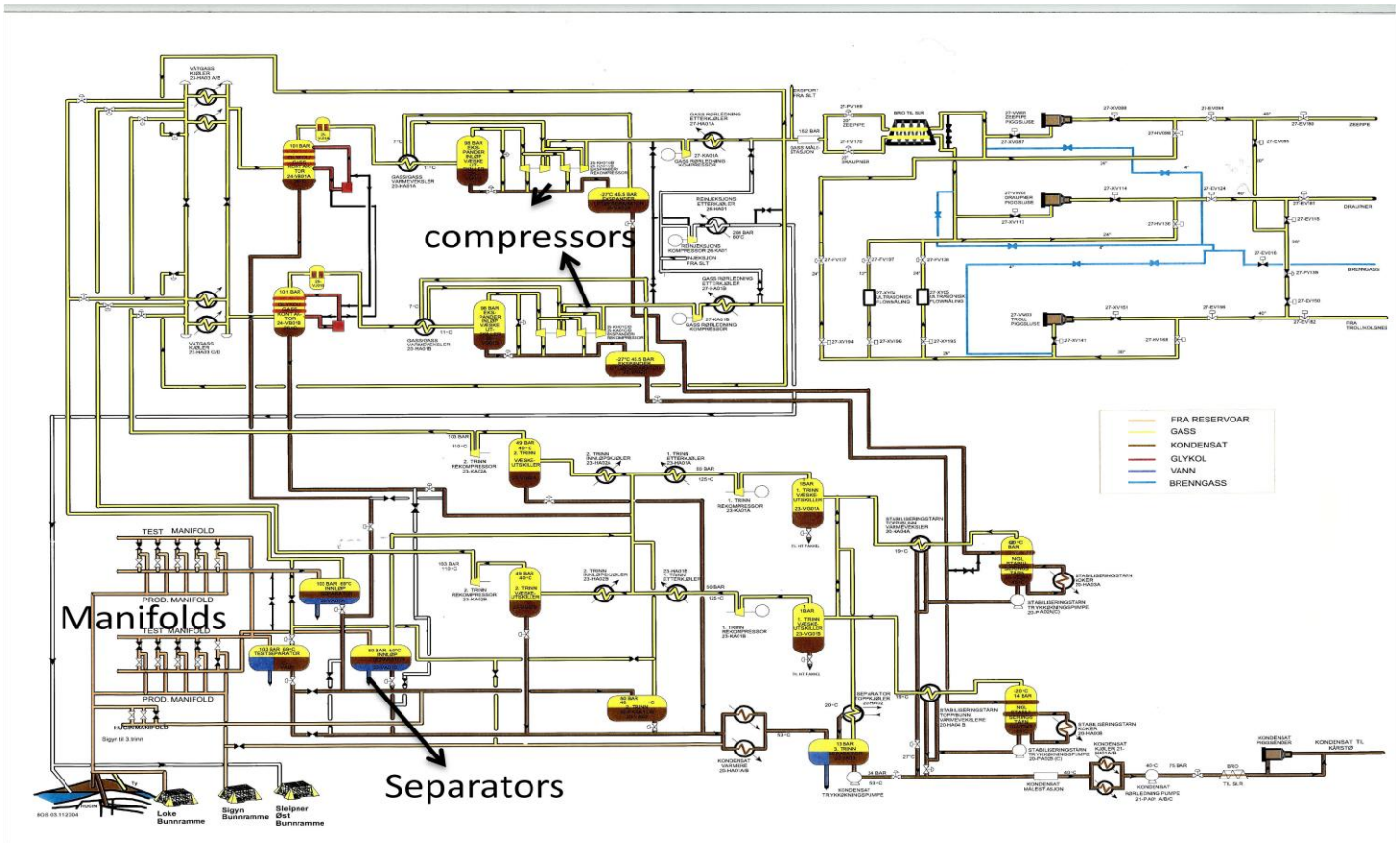

Fig 1 A typical process utility systems network for showing utilities build-up from the reservoir. Highlighted are the manifolds, some separators, and some compressors; these make up a major part of the channels for pressure build up on an offshore production facility.

1.3 Reliefs to flare systems

A flare system consists different relief units that handle depressurization for the different processes taking place on the platform, to ensure safety of life and property on it. Typical sources of process relief are the production manifolds, compression system and separators where it is possible for pressure to build up/overpressure.

The relief systems include; process relief, process flaring, blow-down etc.

Process relief: Process relief involves pressure relief of a process unit in case of overpressure due to a process upset. Overpressure may occur due to heat input which increases pressure through vaporisation and/or thermal expansion; and direct pressure input from higher pressure sources. In order to ensure process safety, pressure relief devices are connected to the vessels and units with a potential for overpressure.

The design basis of these pressure relief devices is dependent on the thermo-hydraulic conditions; pressure, and temperature of the vessel being relieved. These will be taken into account in order to determine the required relieving rate. The design pressure (set pressure) of the relief valve is usually set to a value at which it (the valve) opens to prevent pressure build up above the vessel design pressure.

Process Flaring: Process flaring involves the controlled flaring or bleeding out of gas from a particular process unit or compressor, in case of pressure build up above the acceptable limits. This is in order to allow for continued production, without causing a process upset from build up of pressure. Pressure control valves (PCV or PV) are used for process flaring.

Blow down: Blow down is the actual process of depressurizing a given process unit (separator/piping) after shut down. A blow down valve (BDV) is used. In case of fire out break or related contingencies, the blow down valve opens up (is opened up) to release highly flammable fluids such as hydrocarbons from the separator or piping into the flare network. This serves as a safety measure against escalation of the fire into a full blown explosion.

1.4 The Flare Network

The flare network is a connection of pipes that serve as the pathway for releases during a process relief. Discharged fluid from the relief valves are led through the flare network to a safe disposal point. The disposal system may be single device (connected to only a single relieving device), or multiple device disposal. Flare networks are normally multiple device disposal system due to the economic advantage it presents. The releases are disposed off to a vessel or point of lower pressure than the vessel being relieved. Gaseous releases are disposed off or flared (combusted) to the atmosphere, while liquid/heavier releases are disposed through drains. Below are the main components of a flare network.

- *Tail pipes*
  The tailpipes are connected with the relieving device, PSV or PV, so they are the first contact line of the discharge/flare network. They are of comparably smaller diameters than the other branches of the flare network, and are designed to handle the maximum

allowable back pressure of the relieving device they are connected to. Flow velocities may be very high for tailpipes, they are designed for Mach numbers of up to 0,7.

- *Flare Sub-Headers and Main Header*
  Flare Headers serve as the collection point for releases coming from the different tailpipes. Depending on the size of the disposal system, system loads and back pressure limitations, flare sub-headers may be required as intermediate lines connecting with the main header. Flare headers are of larger diameter than the other network pipes and are designed for Mach number of up to 0,6.
  Flare headers are classified as high pressure or low pressure flare headers based on the pressure range of the incoming streams; typically below 10 bara for low pressure Flare Headers, and above 10 bara for high pressure Flare Headers.

- *Knock-out Drum (KOD)*
  The Knock-out Drum is a separation unit, usually a simple 2-phase separator. The heavy fluids like oil/condensate and water are lead out to drains and often pumped back into the separation system, while the lighter and gaseous components of the stream escape to the flare stack.

- *Flare Stack and Tip*
  The flare stack is usually an elevated pipe pointing upwards. For offshore platforms, the size, positioning and orientation of the flare stack is a function of factors like personnel safety, wind direction, and radiation heat from the burning flare. The flare stack is designed for velocities of up to 0,5 Mach. It is connected to the Flare Tip, which serves as the burner for the combusted gases. For disposal to the atmosphere, the pressure downstream the Flare Tip is atmospheric.

1.5 Flare System Design

A brief discussion on the main design parameters and requirements, regulations/standards

In the design of a flare system several factors have to be taken into consideration; engineering, safety, economic and ethical. A proper analysis of thermal and hydraulic loads resulting from various relief scenarios and process contingences are crucial to sizing the different relief devices and components of the flare network.

To ensure safe and reliable design, there are national and international standards that give guidelines on recommended practice for flare system design:

- NORSOK standard P-100
- NORSOK standard P-001
- NORSOK standard S-001
- API 521/ ISO 23251
- API 520

2 Theoretical basis for thermo-hydraulic modeling of flow in flare systems

2.1 General Fluid flow Equations

All flow problems are solved by applying one or more of the 3 conservation laws; the continuity equation, the energy balance equation, and the momentum balance equation. The general forms of these equations are referred to as the Navier Stokes equations.

Appropriate assumptions and simplifications are applied to these general equations in order to solve specific flow problems. For flow in pipes, the following assumptions may apply

1. One dimensional flow in the axial direction is assumed

2. Steady state flow

The general conservation equations for one dimensional flow may be written as follows:

Continuity Equation:

$$\frac{dm_s}{dt} = \frac{dm_{CV}}{dt} + \frac{dm_{CV}^{out}}{dt} - \frac{dm_{CV}^{in}}{dt} = 0, system\ is\ conserved\ (s\ stands\ for\ system).$$

Since the control volume (CV) is fixed, the accumulation of mass within the control volume

$\frac{dm_{CV}}{dt} = \not{V}\frac{\partial \bar{\rho}_{CV}}{\partial t}$,
$\bar{\rho}_{CV}$ *is the average density within the control volume and can only vary with time.* $\not{V}$ is the control volume.

$$\frac{dm_{CV}^{out}}{dt} = \rho_2 A_2 U_2, \qquad \frac{dm_{CV}^{in}}{dt} = \rho_1 A_1 U_1$$

Therefore, for transient flow

$$\rho_1 A_1 U_1 - \rho_2 A_2 U_2 = \not{V}\frac{\partial \bar{\rho}_{CV}}{\partial t}$$

For steady state flow, $\frac{\partial \bar{\rho}_{CV}}{\partial t}$ = 0. i.e.

$$\rho_1 A_1 U_1 - \rho_2 A_2 U_2 = 0, \quad \rho_1 A_1 U_1 = \rho_2 A_2 U_2 = \rho A U$$

$$\text{Mass flow} = \dot{m} = \rho A U = const \tag{2.1}$$

where: m = mass, ρ = fluid density, A = cross-sectional area, U= flow velocity

Energy balance:

$$\sum_{i=inlets} m_i \left(e + \frac{U^2}{2} + gz + \frac{P}{\rho}\right)_i - \sum_{i=outlets} m_i \left(e + \frac{U^2}{2} + gz + \frac{P}{\rho}\right)_i + \frac{dq}{dt} - \frac{dw}{dt} = \frac{dE}{dt} \quad (2.2a)$$

where $\frac{dE}{dt}$ is the accumulation of energy within the system.

For steady state flow accumulation is always equal to zero, therefore the energy balance equation simplifies to the form

$$\sum_{i=inlets} m_i \left(e + \frac{U^2}{2} + gz + \frac{P}{\rho}\right)_i - \sum_{i=outlets} m_i \left(e + \frac{U^2}{2} + gz + \frac{P}{\rho}\right)_i + \frac{dq}{dt} - \frac{dw}{dt} = 0 \quad (2.2b)$$

where:

e is specific internal energy

p = pressure,

g = gravitational constant

z = elevation,

q = heat

w = work

For gases, e + P/ρ = h the specific enthalpy. Thus the equation may be written as:

$$\sum_{i=inlets} m_i \left(h + \frac{U^2}{2} + gz\right)_i - \sum_{i=outlets} m_i \left(h + \frac{U^2}{2} + gz\right)_i + \frac{dq}{dt} - \frac{dw}{dt} = 0 \quad (2.2c)$$

The expression may be further simplified depending on the type of thermodynamic system assumed.

Momentum Balance:

From Newton's second law

$$\sum \boldsymbol{F} = \frac{\mathrm{d}(\mathrm{m}\boldsymbol{U})_{\boldsymbol{s}}}{\mathrm{dt}} = \frac{\mathrm{d}(\mathrm{m}\mathbf{U})_{\mathrm{cv}}}{\mathrm{dt}} + \frac{\mathrm{d}(\mathrm{m}\mathbf{U})^{\mathrm{out}}{}_{\mathrm{cv}}}{\mathrm{dt}} - \frac{\mathrm{d}(\mathrm{m}\mathbf{U})^{\mathrm{in}}{}_{\mathrm{cv}}}{\mathrm{dt}} \quad (2.3)$$

For unsteady state flow there would be accumulation of momentum $\left(\frac{\mathrm{d}(\mathrm{m}\mathbf{U})_{\mathrm{cv}}}{\mathrm{dt}}\right)$ within the control volume, so:

$$\sum \boldsymbol{F} = \frac{\mathrm{d}(\mathrm{m}\mathbf{U})_{\mathrm{cv}}}{\mathrm{dt}} + \frac{\mathrm{d}(\mathrm{m}\mathbf{U})^{\mathrm{out}}{}_{\mathrm{cv}}}{\mathrm{dt}} - \frac{\mathrm{d}(\mathrm{m}\mathbf{U})^{\mathrm{in}}{}_{\mathrm{cv}}}{\mathrm{dt}} \quad (2.4)$$

For steady state flow there is no accumulation of momentum within the control volume, $\frac{d(m\mathbf{V})_{cv}}{dt}=\mathbf{0}$, so:

$$\sum \boldsymbol{F} = \frac{d(m\mathbf{U})^{out}{}_{cv}}{dt} - \frac{d(m\mathbf{U})^{in}{}_{cv}}{dt} \qquad (2.5)$$

But $\frac{d(m\mathbf{U})_i}{dt} = \frac{dm_i}{dt}\mathbf{U}_i = \dot{m}\mathbf{U}$, **i.e** $\sum \boldsymbol{F} = (\dot{m}\mathbf{U})^{\boldsymbol{out}} - (\dot{m}\mathbf{U})^{\mathbf{in}}$ (2.6)

This may be rewritten in scalar form as:

$$\sum F_z = (\dot{m}U_z)^{\boldsymbol{out}} - (\dot{m}U_z)^{\mathbf{in}}$$

$$\sum F_\Theta = (\dot{m}U_\Theta)^{\boldsymbol{out}} - (\dot{m}U_\Theta)^{\mathbf{in}}$$

$$\sum F_r = (\dot{m}U_r)^{\boldsymbol{out}} - (\dot{m}U_r)^{\mathbf{in}} \qquad (2.7)$$

Here $\sum \boldsymbol{F}$ is the sum of all forces acting on the fluid mass, including gravity forces, shear forces, and pressure forces. This can be shown using the Navier-Stocks equations.

2.2 Thermodynamics

A pipe network is also a thermodynamic system; therefore processes occurring in a pipe network during fluid flow may be described using equations of state, thermodynamic laws and relations. Important thermodynamic relations include; enthalpy, entropy, heat capacity.

The equations of State

General equation of state:

$$f(p, v, T) = 0$$

or

$$\frac{pv}{RT} = \frac{p}{\rho RT} = \not{z} \tag{2.8}$$

Where $\not{z}$ is the compressibility factor and R is the gas constant.

For a thermally perfect (ideal) gas, $\not{z} = 1$. Thus the equation of state for a thermally perfect gas becomes:

$$\frac{p}{\rho} = RT \;\; or \; p = \rho RT \tag{2.9}$$

For a thermally imperfect (real) gas $\not{z}$ is a function of temperature and pressure. There exist a number of equations of state for a thermally imperfect (real) gas, the most common of which are:

a) Van der Waal's equation of state:
$P = \frac{RT}{\upsilon - b} - \frac{a}{\upsilon^2}$

b) SRK equation of state:
$P = \frac{RT}{\upsilon - b} - \frac{a_c \alpha}{\upsilon(\upsilon + b)}$
Where
$a_c = f(P_c, T_c)$, $\alpha = (1+S[1-T_r^{0,5}])^2$, $S = 0{,}480+1{,}574\omega-0{,}176\omega^2$

c) Peng Robinson equation of state:
$P = \frac{RT}{\upsilon - b} - \frac{a_c \alpha}{\upsilon(\upsilon + b) + b(\upsilon - b)}$
Where
$S = 0{,}37464+1{,}5422\omega-0{,}26992\omega^2$,
P = pressure, T= temperature, R = Universal gas constant, υ = volume, a, b = f(P,T),
ω = acentric factor

The Peng Robinson EOS gives a more accurate estimation of the liquid phase density in VLE calculations.

Laws of thermodynamics

The first law of thermodynamics:

It is a statement of the principle of conservation of energy.

$$de = dq + dw = dq - pdv \tag{2.10}$$

The second law of thermodynamics:

It states that for a closed system (one in which neither heat nor work is exchanged with the surroundings) the entropy remains constant or increases but never decreases.

$$Tds = de + pdv = dq \tag{2.11}$$

$$ds = \frac{dq}{T} \tag{2.12}$$

where s = entropy

Some general thermodynamic relations

Heat capacities:

$$c_v = \left(\frac{\partial e}{\partial T}\right)_v$$

$$c_p = \left(\frac{\partial q}{\partial T}\right)_p$$

for a thermally perfect (ideal) gas

$$c_p = c_v + R \tag{2.13}$$

where: c_p/c_v = constant pressure/volume specific heat capacity

Specific enthalpy:

$$h = e + pv \tag{2.14}$$

for a thermally perfect (ideal) gas

$$h = e + RT$$

$$dh = de + RdT = c_v dT + RdT$$

$$dh = (c_v + R)dT = c_p dT \tag{2.15}$$

2.3 Different flow considerations

Depending on if the density/volume of a fluid is a function of temperature and pressure or not, flow may be considered compressible or incompressible.

2.3.1 Incompressible flow

For steady state incompressible flow density is constant. This largely simplifies the conservation laws, as compressibility effects are neglected. The conservation equations take the form:

Continuity Equation:

$$Q = AU = const \tag{2.16}$$

Energy Equation:

$$\left(\frac{p}{\rho g} + \frac{U^2}{2g} + z\right)_{in} = \left(\frac{p}{\rho g} + \frac{U^2}{2g} + z\right)_{out} + h_L \tag{2.17}$$

where: $h_L = \frac{\Delta p_0}{\rho g}$, head loss

Momentum Equation:

$$\sum F = (\rho QU)_{out} - (\rho QU)_{in}$$

Or stream force

$$I = (p + \rho U^2)A \tag{2.18}$$

Here Q = volumetric flow rate

2.3.2 Compressible flow

Compressible flow is flow of gas, or vapor. Fluid properties such as density and volume are a function of temperature and pressure. This strongly influences the flow behavior. Appropriate equations of state and thermodynamic relations are used to characterize the flow parameters/behavior.

For compressible flow, the energy equation takes the form

$$h_1 + \frac{U_1^2}{2} + q_H = h_2 + \frac{U_2^2}{2} \tag{2.19}$$

where q_H is heat gained or lost.

2.3.2.1 Speed of sound; Mach number

According to [3], the speed of sound is defined as that speed at which an infinitesimal disturbance is propagated in a uniform medium initially at rest. It is assumed to be characterized by isentropic conditions.

Speed of sound is given as

$$c^2 = \frac{\gamma p}{\rho} = \gamma RT = \frac{\gamma R_0 T}{M_w} \qquad (2.20)$$

γ = specific heat ratio, R = individual gas constant, R_0 = universal gas constant, M_w = molecular weight

The Mach number, M is the ratio of the local velocity to the local speed of sound

$$M = \frac{U}{c} \qquad (2.21)$$

When M<1, the flow is subsonic; when M=1, the flow is sonic; for M>1 the flow is said to be supersonic.

Mach number is a parameter strictly related with compressible flow. Mach number does not exist in incompressible flow (M=0), because the speed of sound is considered infinite in this case.

Mach number serves as a valuable parameter in describing compressible flow. At low Mach numbers, M <= 0,3 gas or vapor flow may be described with the assumption of incompressibility; with minimal error in the estimation of flow properties.

2.3.2.2 Adiabatic Flow

In adiabatic flow there is no heat transfer, $q_H = 0$. The energy balance equation takes the form

$$h + \frac{U^2}{2} = const \qquad (2.22)$$

since for a perfect gas

$$h = c_p T \qquad (2.23)$$

the energy equation may be written as

$$c_p T + \frac{U^2}{2} = const \qquad (2.24)$$

$$c_p T_1 + \frac{U_1^2}{2} = c_p T_2 + \frac{U_2^2}{2} = c_p T_0 \qquad (2.25)$$

Here T_0 is the stagnation temperature, the temperature at static conditions (U = 0). This holds for holds for adiabatic flow with or without friction.

For adiabatic frictional flow (Fanno flow) in a constant area duct, the energy equation can be rederived to give an expression for the pressure drop as

$$f\frac{L}{D}\frac{1}{2}\left(\frac{\dot{m}}{A}\right)^2 = -\int_1^2 \rho dp - \left(\frac{\dot{m}}{A}\right)^2 ln\frac{\rho_1}{\rho_2} \qquad (2.26)$$

In adiabatic frictional flow critical conditions occur at M=1. The maximum flow speed which is the speed of sound is reached, and this occurs downstream of the pipe.

An illustration of adiabatic frictional flow behavior – the Fanno line – has been included as attachment.

2.3.2.3 Isothermal Flow

Temperature, T is said approximately constant in isothermal flow. In this case the internal energy and enthalpy remain constant. The energy balance equation takes the form:

$$\frac{U_1^2}{2} + q_H = \frac{U_2^2}{2} \qquad (2.27)$$

For frictional flow in a pipe of uniform diameter, the energy balance equation may be rederived to give an expression for the pressure drop for isothermal flow across a pipe of constant cross-section

$$p_1^2 - p_2^2 = \frac{\dot{m}^2 RT}{A^2}\left(f\frac{L}{D} + 2ln\frac{p_1}{p_2}\right) \qquad (2.28)$$

In terms of Mach number

$$\frac{M_1^2}{M_2^2} = 1 - \gamma M_1^2\left(f\frac{L}{D} + 2ln\frac{M_2}{M_1}\right) \qquad (2.29)$$

where $M_2/M_1 = p_1/p_2$

There is a limiting factor on how large the velocity can get of $M = 1/\sqrt{\gamma}$. The pressure drop equations are applicable for $M < 1/\sqrt{\gamma}$.

[1] Includes a comparison between adiabatic flow and isothermal flow of air through a constant area duct, assuming the same initial values for each. Inspection of the results showed that at low pressure drops, $p_2/p_1 > 0{,}9$, showed very little difference (see Appendix C). Thus adiabatic flow in a pipe may be analyzed as isothermal flow without introducing much error, for such pressure drop ranges.

2.3.2.4 Mach number relationships

Pressure and Temperature variation in pipe flow can be expressed in relation to the Mach number of the flow. Depending on the upstream and downstream Mach numbers, the other flow parameters may be related as follows:

1) *Flow through a nozzle, convergent; divergent; convergent/divergent nozzles (Valves and Orifices)*
   The general relationship relating the influence of cross-sectional area change on flow speed is given as

$$\frac{dU}{U} = -\frac{1}{(1-M^2)}\frac{dA}{A} \qquad (2.30)$$

$$\frac{dM}{M} = -\frac{\left\{1+\frac{\gamma-1}{2}M^2\right\}}{(1-M^2)}\frac{dA}{A} \qquad (2.31)$$

   These relations shows that
   a) At subsonic speeds, 0<=M<1, an increase in area gives rise to a decrease in flow velocity and Mach number, and vice versa.
   b) At supersonic speeds, M>1, an increase in area gives rise to an increase in velocity and Mach number; and a decrease in area gives rise to a decrease in velocity and Mach number.
   c) At sonic velocity, M=1, the denominator (1- M^2) is zero. This means that for the axial change in velocity and Mach number (dU/dx and dM/dx) not to become infinite, the axial change in cross-sectional area (dA/dx) must be zero; i.e. cross-sectional area must be constant at M=1.

From the analysis above, it can be stated that an initially subsonic flow through a convergent - divergent nozzle will remain subsonic if it does not turn sonic at the throat.

2) *Flow through a constant area duct (pipe segements)*

Normal shock waves: [2] defines the following relationship for adiabatic flow through a duct of constant cross-sectional area, in which discontinuity of flow properties exist due to the presence of a normal shock wave.

The conditions on either side of the discontinuity may be related by applying the principles of conservation of continuity, momentum, and energy as below

$$\rho_1 U_1 = \rho_2 U_2 ,$$

$$p_1 + \rho_1 U_1^2 = p_2 + \rho_2 U_2^2 ,$$

$$h_1 + \frac{U_1^2}{2} = h_2 + \frac{U_2^2}{2} = h_0 .$$

(2.32)

Writing these equations for a perfect gas, for which $h = C_P T$; the energy equation then shows that the total temperature, T_0 remains constant across a normal shock wave.

Using the relations for a perfect gas, and the definition of Mach number, the conservation equations take the form

$$\frac{T_1}{T_2} = \left(\frac{p_1}{p_2}\right)^2 \left(\frac{M_1}{M_2}\right)^2 ,$$

$$\frac{p_1}{p_2} = \frac{1 + \gamma M_2^2}{1 + \gamma M_1^2},$$

and

$$\frac{T_1}{T_2} = \frac{1 + \frac{\gamma - 1}{2} M_2^2}{1 + \frac{\gamma - 1}{2} M_1^2}.$$

(2.33)

Eliminating temperature and pressure from these 3 relationships and solving for M_2 in terms of M_1, we have

$$M_2 = \left[\frac{2 + (\gamma - 1)M_1^2}{2\gamma M_1^2 - (\gamma - 1)}\right]^{\frac{1}{2}} \qquad (2.34)$$

In practice it is seen that that the condition; if $M_1 > 1$, then $M_2 < 1$ holds, while for $M_1 < 1$, M_2 is limited to a maximum value of 1.

It is said that M_1 can have any value in the range $0 \leq M_1 \leq \infty$. Inspection of the equation above shows that the minimum value of M_2 is $[(\gamma-1)/2\gamma]^{1/2}$, corresponding to M1 = ∞. So the possible range of M_2 is $[(\gamma-1)/2\gamma]^{1/2} \leq M_2 \leq 1$.

Based on the equations above, pressure, temperature and density ratio relationships across a normal shock in terms of M_1 or M_2 may be written, results which may be summarized as

a) M, U, p_0 decrease;
b) T_0 remains constant;
c) P, T, ρ, s, and a increase
   when the flow passes through a shock wave.

Stagnation properties

A relationship between stagnation properties (at zero velocity) and static properties may be expresses in terms of Mach number

$$\frac{T_0}{T} = 1 + \frac{\gamma-1}{2}M^2 \qquad (2.35)$$

$$\frac{p_0}{p} = \left(1 + \frac{\gamma-1}{2}M^2\right)^{\gamma/(\gamma-1)} \qquad (2.36)$$

2.3.3 Multi-phase flow

Simultaneous flow of oil, gas, and water is common in oil and gas installations. Pressure drop and flow behavior in multi-phase flow strongly differs from single phase flow, and thus cannot be well defined by single phase flow models. Multi-phase flow is associated with higher pressure drops; flow regimes are strongly influenced by pipe dimension and inclination, and flow-rate of the different phases. There are a number of multi-phase flow pressure drop and friction factor correlations and models available today. Some of them are listed below

- The Beggs and Brill model
- The Lockhart-Martinelli correlation
- The Taitel and Dukler model
- The BTD model for vertical upward flow
- Oresweski model for vertical flow

None of these models is thought to be universal, covering all flow regimes and fluid properties encountered in multi-phase flow. These multi-phase flow pressure drop correlations are used in numerical simulators. A number of them are available for use in FlareNet. A brief description of the Beggs and Brill model is presented below.

2.3.3.1 The Beggs and Brill pressure drop model

H. D. Beggs and J. P. Brill developed pressure drop correlations for 2-phase (gas/liquid) flow using air and water. The parameters studied and their range include

1. Gas flow rates of (0 to 300Mscf/D), liquid flow rates of (0 to 30 gal/min)
2. Pipe diameter of (1 to 1.5 inch)
3. Inclinations angles of (-90^o to +90^o) from the horizontal

The 2-phase flow regimes were divided into 4 groups, limited within ranges for certain derived parameters.

- Segregated flow

$$\lambda_L < 0.01 \; and \; N_{FR} < L_1$$
$$Or \; \lambda_L \geq 0.01 \; and \; N_{FR} < L_2$$

- Transitional flow

$$0.01 \leq \lambda_L \; and \; L_2 \leq N_{FR} \leq L_3$$

- Intermittent flow

$$0.01 \leq \lambda_L < 0.4 \; and \; L_3 < N_{FR} \leq L_1$$
$$Or \; \lambda_L \geq 0.4 \; and L_3 < N_{FR} \leq L_4$$

- Distributed flow

$$\lambda_L < 0.4 \; and \; N_{FR} \geq L_1$$
$$Or \; \lambda_L \geq 0.4 \; and \; N_{FR} \geq L_4$$

Where:

$$N_{FR} = \frac{U_{mix}^2}{gD}, Froude\ number$$

$$\lambda_L = \frac{U_{LS}}{U_{GS}}, input\ liquid\ content$$

$$L_1 = 316 * \lambda_L^{0.302}$$

$$L_2 = 9.52 * 10^{-4} * \lambda_L^{-2.4684}$$

$$L_3 = 0.1 * \lambda_L^{-1.4516}$$

$$L_4 = 0.5 * \lambda_L^{-6.738}$$

It is noteworthy that this correlation is not limited by inclination. It is applicable to horizontal, inclined and vertical 2-phase gas-liquid flow in pipes.

The Beggs and Brill (homogeneous) model is the recommended pressure drop model for use in FlareNet for cases of multi-phase flow

2.3.3.2 Speed of Sound in Multi-phase (gas-liquid) flow

For cases with gas-liquid flow (partial condensation of gas or vaporization of liquid phase) the speed of sound and thus Mach number will be strongly affected. Speed of sound lies in the range of 300m/s in gas, and over 1000m/s in liquid. But for gas-liquid flow the speed of sound depends on the flow regime, and phase fraction. Below is a figure taken from [4] showing the effect gas-liquid flow on the speed of sound for water (c = 1500 m/s) and gas (c = 344m/s). Two extreme gas-liquid flow regimes are considered; stratified flow and homogenized flow.

For stratified flow speed of sound is given as

$$c_S = \left[\frac{\frac{\epsilon_G}{\rho_G} + \frac{\epsilon_L}{\rho_L}}{\frac{\epsilon_G}{\rho_G c_G^2} + \frac{\epsilon_L}{\rho_L c_L^2}}\right]^{1/2}$$

where: ϵ_G and ϵ_L are gas and liquid phase fractions,

c_G and c_L are sound speed in gas and liquid,

ρ_G and ρ_L are gas and liquid phase densities

In homogenized (dispersed) flow speed of sound is given as

$$c_H = \left[(\epsilon_G * \rho_G + \epsilon_L * \rho_L) * \left(\frac{\epsilon_G}{\rho_G c_G^2} + \frac{\epsilon_L}{\rho_L c_L^2}\right)\right]^{-1/2}$$

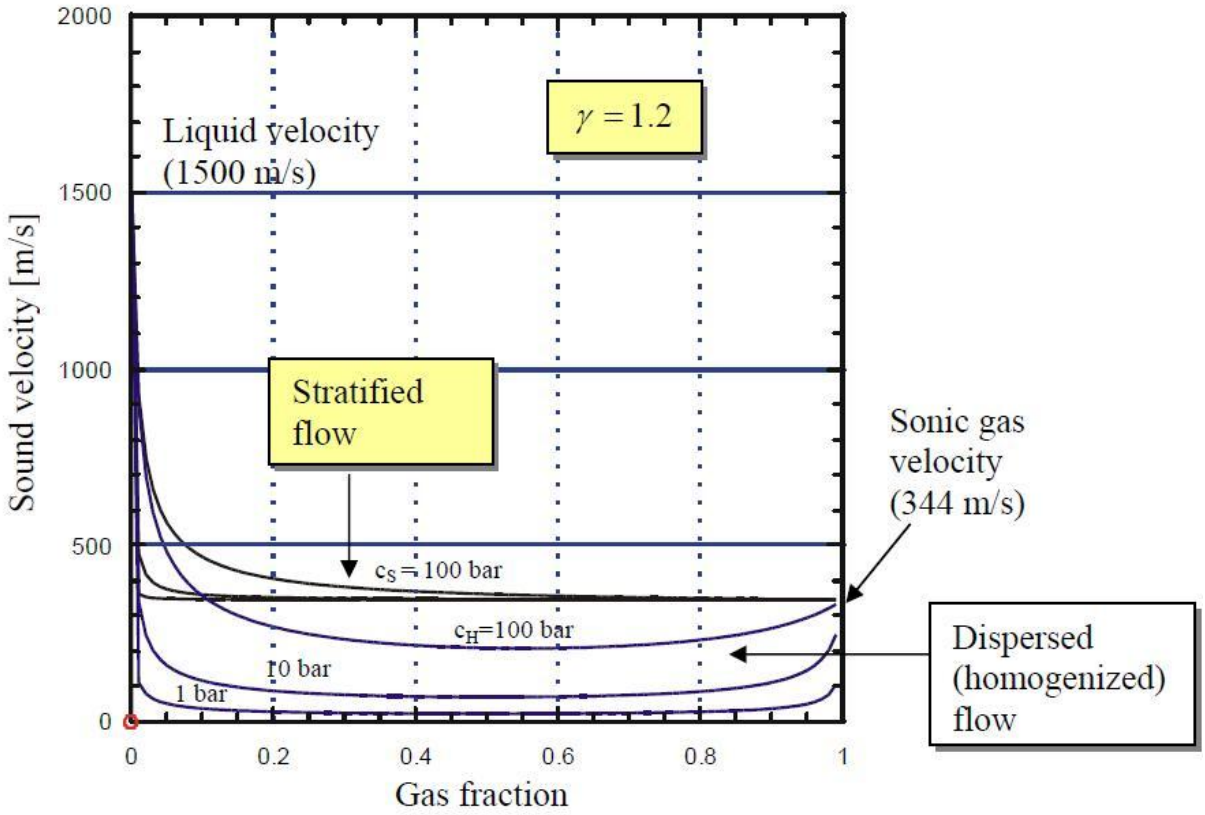

Fig 2.3.3.2 Sonic velocity in gas-liquid flow, for stratified {black line} and homogenized (dispersed) {blue line} flow. Plots are shown for pressures of 1, 10 and 100 bar.

The plots show that gas-liquid sonic velocity for homogenized flow (typical to flare systems) is nearly always lower than the individual sonic velocity gas and liquid phases.

2.4 Additional pressure loss in fluid flow (Flow through tees, bends, expansions/contraction)

Considering flow through a Tee joint as described below:

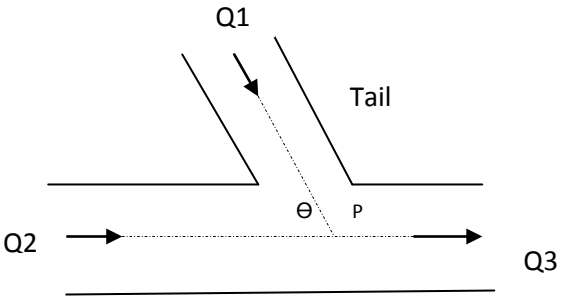

We shall consider combining or mixing flow, which is typical for a flare network.

Continuity equation:

$$Q1 + Q2 = Q3$$

Energy Balance:

$$\left(\mathrm{p} + \frac{1}{2}\rho \mathrm{U}^2 + \rho \mathrm{gz}\right)_{\boldsymbol{in}} - \left(\mathrm{p} + \frac{1}{2}\rho \mathrm{U}^2 + \rho \mathrm{gz}\right)_{\boldsymbol{out}} = \Delta \mathrm{p}_{\mathrm{in-out}}$$

Where $\Delta \mathrm{p}_{\mathrm{in-out}}$ is the loss in total pressure.

Momentum Balance:

Let's say the piezometric is given as $\hat{p} = p + \rho g z$, then:

$$(\hat{p}_1 + \rho_1 U_1^2 cos\theta)A_1 + (\hat{p}_2 + \rho_2 U_2^2)A_2 = (\hat{p}_3 + \rho_3 U_3^2)A_3$$

[2]

When two flows meet at a junction, there is an additional loss in pressure due to:

1) Obstruction to flow caused by the junction
2) The formation of eddies as a result of mixing of the 2 streams

[2]

To account for the pressure loss across Tees/junctions/branches, restrictions and bends, pressure loss coefficients and resistance coefficients are used.

2.4.1 Pressure loss coefficients

According to [2] the pressure loss coefficient is determined separately for each incoming stream in relation to the outgoing stream and is given as:

$$K_{13} = \frac{\Delta p_{13}}{\frac{1}{2}\rho U_3^2} \qquad (2.37)$$

$$K_{23} = \frac{\Delta p_{23}}{\frac{1}{2}\rho U_3^2} \qquad (2.38)$$

The loss coefficients have been defined using the total pressure drop across the branches and the dynamic pressure in the branch with the combined flow.

By solving simultaneously the continuity equation, energy balance equation and momentum balance equation, we get an expression for K as a quadratic function of Q1/Q3, dependent on the ratio A3/A1 and on the angle Θ.

In line with this loss coefficients were experimentally obtained, and empirical correlations were developed to match the experimental data. Among these are correlations by Gardel (1957) and Miller (1971). The experiments were conducted under turbulent flow conditions in the range of (Re) = 10^5.

For flow through 90^o-junctions, with A_1=A_2=A_3 and q=Q1/Q3; Gardel (1957) gives the following correlating equations

$$K_{13} = -0.92(1-q)^2 + q(1-q) + 1.2q^2 \qquad (2.39)$$

and

$$K_{23} = 0.03(1-q)^2 + q - 0.38q^2 \qquad (2.40)$$

Miller's (1971) experimental data best fit the empirical relations given by Ito and Imai (1973)

$$K_{13} = 1.09 - 0.53(1-q) - 1.48(1-q)^2 \qquad (2.41)$$

and

$$K_{23} = 0.045 + 1.38q - 0.90q^2 \qquad (2.42)$$

[2]

Influence of geometric parameters

Taking into account the influence of inclination, Θ, and cross-sectional area ratio A1/A3 (given A2=A3), and the radius ρ, of a fillet used by Gardel to fair the tail limb 1, into the main. A group of tests were run with $\Theta=90^{o}$, and varying A1/A3 in the range $0.4<A1/A3<1$; for A1=A2=A3 and vary Θ in the range $45^{o}<\Theta<135^{o}$; and for r, varied in the range $0.02<r<0.12$, where $r=\rho/D_3$.

The empirical equations derived by Gardel to fit the results from these experiments were:

$$K_{13} = -0.92(1-q)^2 - q^2\left[\left(1.2 - r^{\frac{1}{2}}\right)\left(\frac{cos\theta}{a} - 1\right) + 0.8\left(1 - \frac{1}{a^2}\right) - \left(\frac{1}{a} - 1\right)cos\theta\right] + (2-a)(1-q)q,$$

$$K_{23} = 0.03(1-q)^2 - q^2\left[1 + \left(1.62 - r^{\frac{1}{2}}\right)\left(\frac{cos\theta}{a} - 1\right) - 0.38(1-a)\right] + (2-a)(1-q)q \quad (2.43)$$

Where

$$a = {}^{A_1}/_{A_3}$$

[2]

2.4.2 Resistance Coefficients

For fluid flow through bends and restrictions like valves and fittings, there also is additional pressure loss due to one or more of the following reasons:

1) Changes in direction of flow path
2) Obstructions in flow path
3) Sudden or gradual changes in the cross-section and shape of flow path
4) Loss due to curvature (for bends)
5) Excess loss in the downstream tangent (for bends)

According to [3]; velocity in a pipe is obtained at the expense of static head, and decrease in static head due to velocity is,

$$h_L = \frac{U^2}{2g}$$

which is also defined as he "velocity head". Flow through a restriction similarly causes a reduction in static head that may be expressed in terms of the velocity head. In this case,

$$h_L = K\frac{U^2}{2g} \qquad (2.44)$$

Where K is the resistance coefficient; defined as the number of velocity heads lost due to a restriction. The resistance coefficient is considered as being independent of friction factor or Reynolds number, and may be treated as a constant for any given restriction in a piping system under all conditions of flow.

If the formula for h_L above is compared with that for a strait pipe,

$$h_L = \left(f\frac{L}{D}\right)\frac{U^2}{2g}$$

then

$$K = \left(f\frac{L}{D}\right) \qquad (2.45)$$

Where L/D is the equivalent length in pipe diameters of a straight pipe, that will cause the same pressure drop as the given obstruction under the same flowing conditions.

In bends, the additional head loss may be split into 3 component part given as:

$$h_t = h_p + h_c + h_L \qquad (2.46)$$

Where:

h_t = total loss

h_p = excess loss in downstream tangent

h_c = loss due to curvature

h_L = loss in bend due to length

Losses due to curvature and downstream tangent can be summed to give a quantity $h_b = h_p + h_c$, that can be expressed as a function of velocity head in the formula:

$$h_b = K_b\frac{U^2}{2g} \qquad (2.47)$$

Where:

K_b is the bend coefficient.

Taking the additional losses into consideration, the energy balance for fluid flow through a pipe with bends and restrictions may be written as follows:

$$\frac{p_{in} - p_{out}}{\rho g} + \frac{U_{in}^2 - U_{out}^2}{2g} + z_{in} - z_{out} = h_L + h_t \qquad (2.48)$$

and

$$h = h_L + h_t$$

where:

h = total head loss

hL = loss due to pipe length

ht = additional loss due to restriction

then

$$h = \left(f\frac{L}{D} + K + K_b\right)\frac{U^2}{2g} \qquad (2.49)$$

U is the flow velocity (usually downstream) through the restriction.

Several experiments have been conducted for the evaluation of K and Kb for different restriction types; values which can be found in standard tables and charts.

Comparing equations (2.37), (2.38) with (2.44) we see that pressure loss coefficients and resistance coefficients are derived from the same expression. Therefore correctly estimated resistance coefficients should give the same value for pressure loss as the pressure loss coefficients used in tee correlations.

3 Simulation tools used

Two simulation tools where used in the simulations, FlareNet, OLGA. The simulations were first to be run in FlareNet, a simulation tool designed specifically for flare system design and that has been the main tool used at Aker solutions MMO Stavanger for such work; subsequent identical runs were done in OLGA. The results where then compared with FlareNet, for steady state conditions.

3.1 Modeling in FlareNet

Aspen Flare Systems Analyzer (FlareNet) from **Aspen Tech** is a steady state simulation tool specifically tailored for flare system design. It is used for design phase work such as line sizing, valve sizing; for simulating different relief scenarios, blow-down, debottlenecking, and other modifications.

Building a model in FlareNet is simple and straightforward, with in-built materials commonly used for flare system design. FlareNet provides several options of traditional flow simulation models and correlations for pressure drop calculations, additional fittings loss calculation for bends and restrictions, tee pressure loss correlations, and equations of state, among others. Available pressure drop models include those for single phase gas flow and multi-phase flow such as; Isothermal flow, Adiabatic gas flow, Beggs&Brills, Taitel&Duckler, Lockhart Martinelli e.t.c. ; tee correlations such as: Miller's correlation, Gardel's correlation; equations of state include: compressible gas, SRK, Peng Robinson.

FlareNet gives the opportunity to built a flare system model and simulate within the boundaries of accepted guidelines and standards (API, NORSOK, ISO), by specifying system constraints such as; allowable Mach within the different lines, from tailpipes to flare stack, noise, radiation, allowable back-pressure.

Input parameters are usually; fluid composition (can be imported from Aspen HYSYS), pipe type with size (Carbon Steel or Stainless Steel, pipe inner diameter and roughness) and geometry (length and elevation). Pressure and Temperature upstream the relief and blow-down valves, and relieving rates (mass flow rate). Ambient conditions are also specified, with atmospheric conditions downstream the flare tip.

FlareNet estimates the system variables (temperature and pressure in the pipe system and reports results for inlet end (upstream) and outlet end (downstream) of each pipe segment/section, and line sizes[diameters]), based on input data and system constraints. The pressure and temperature (corresponding to inlet temperature and heat balance along pipe system) is first estimated starting from the flare tip, backwards to upstream the tailpipes; then the lines are sized in the opposite direction from upstream tailpipes to the flare tip, based on estimated flow parameters (This is an iterative process).

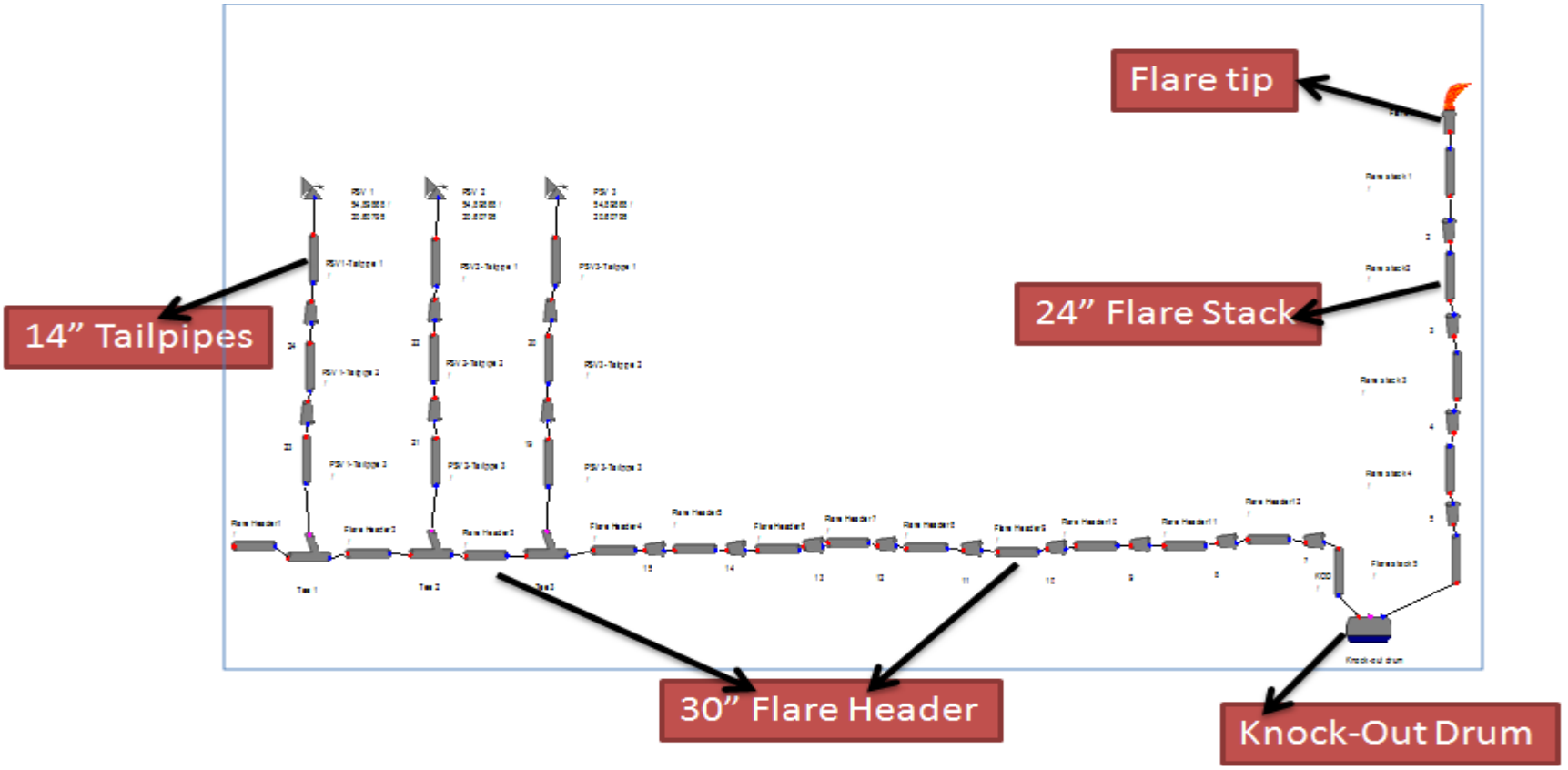

Fig 3.1 Flare network model view in FlareNet

3.2 Modeling in OLGA

OLGA from SPT group, is a well known and widely used flow simulation tool with many options of application from well flow to riser and pipeline flow simulation. OLGA can be run in both steady state and dynamic mode, making it a good tool for simulating the many time dependent processes faced in the industry.

Building the model in OLGA though generally needs more input variables to be specified by the user than for FlareNet; line/pipe wall material and properties, amongst others. Pressure drop, thermodynamic properties and other flow parameters are calculated based on generally accepted theory (no detailed information on this), the basic conservation equations and other in-house correlations. Calculation options are tailored to match the flowing fluid type; GAS/LIQUID, HYDROCARBON/WATER, Single phase/2-phase/3-phase. Simulation runs might be comparably more time consuming than FlareNet since Olga is a dynamic simulation tool (i.e. Calculations are done in time steps).

It is our assumption that the correlations used in OLGA are within normal pipeline and well flow limits. Agreeably the fundamental fluid dynamics and thermodynamic relations as used in OLGA may have no known limits, but we are interested in seeing if OLGA can reasonably simulate and estimate flow parameters for flare networks at the high flow rates/velocities in flare systems, under steady state conditions.

To compare with FlareNet, the PSV was represented by a closed node and a source upstream the tailpipe, with pressure (Maximum allowable back pressure) and temperature specified. Tees are represented by internal nodes. There are no tee or fittings correlations ; therefore additional pressure loss due to restrictions, tees and valves may be added using (calculated) loss coefficients. For single phase gas flow, the Knock-Out drum was represented by a pipe segement having corresponding geometry as was the case in FlareNet. The Flare Tip was represented by a valve modelled as an orifice valve, with C_V value adjusted to give a pressure drop that matches the given flare tip pressure drop curve. *Note: in FlareNet a knock-out drum generally has no volume, since it is more a kind of a phase splitter (to remove liquid before the gas enters the flare stack). In Olga the KOD may be modelled as a real separator with a volume (length, diameter).*

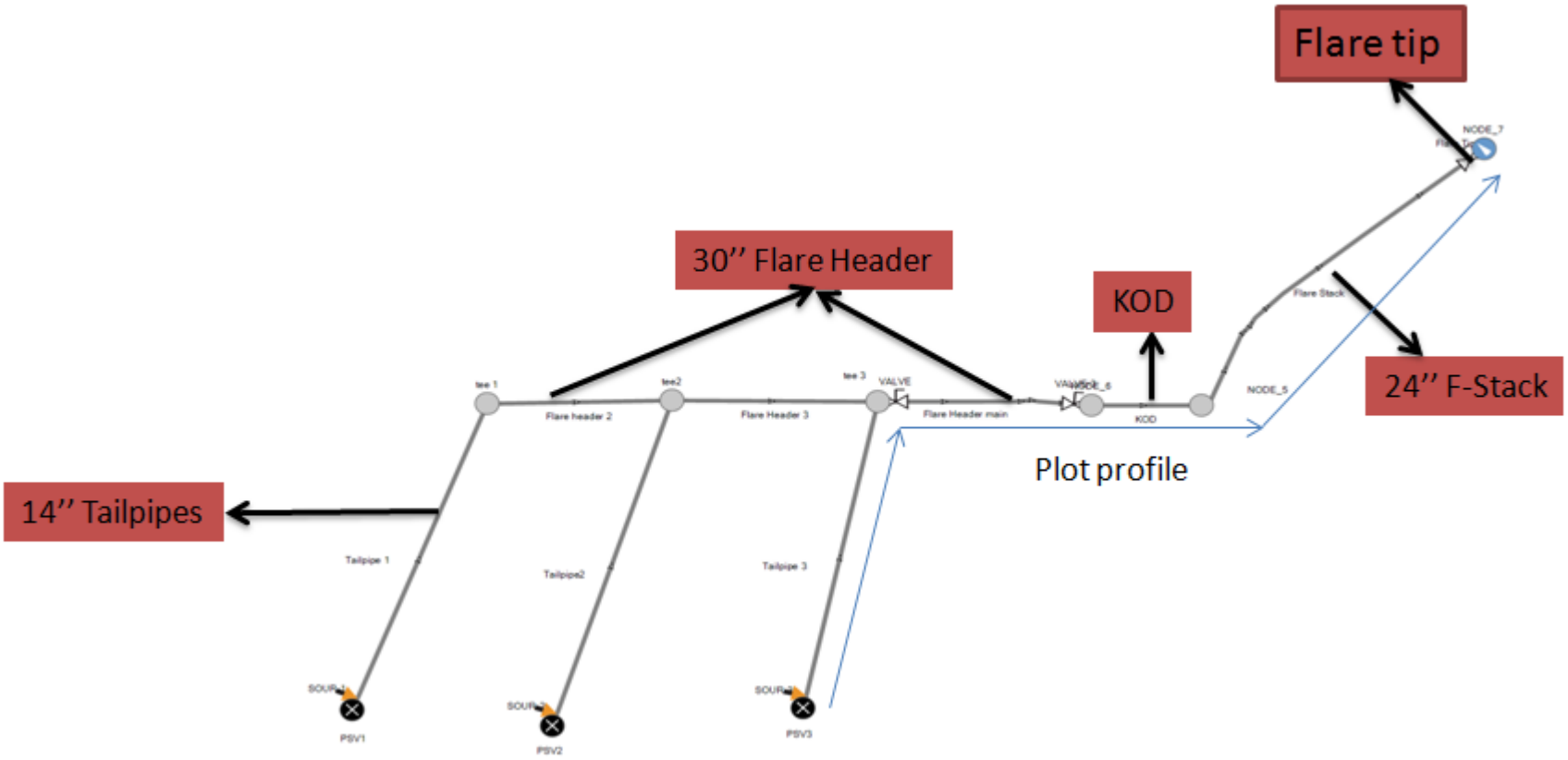

Fig 3.2 Flare network model view in OLGA, thin arrows showing flow path for which result plots were made

4 Cases Studied

As part of the project aims several cases were looked at within FlareNet. Individual simulation runs were done for comparing between the different pressure drop models, tee correlations, and friction factor correlations.

Simulation results from FlareNet for a chosen pressure drop model was then to be compared with results from the other simulation tools; OLGA/HYSYS.

The reason for the studies in FlareNet was to verify that the proposed models in the tool worked in agreement with established theory on which they are based, and gaining a clearer understanding on how the tool works.

As mentioned earlier, OLGA and HYSYS are both steady sate and dynamic tools. Comparing the FlareNet results with the results from OLGA/HYSYS under steady state conditions would give a baseline for establishing if the results from OLGA/HYSYS under dynamic conditions can be considered as reliable.

System Overview

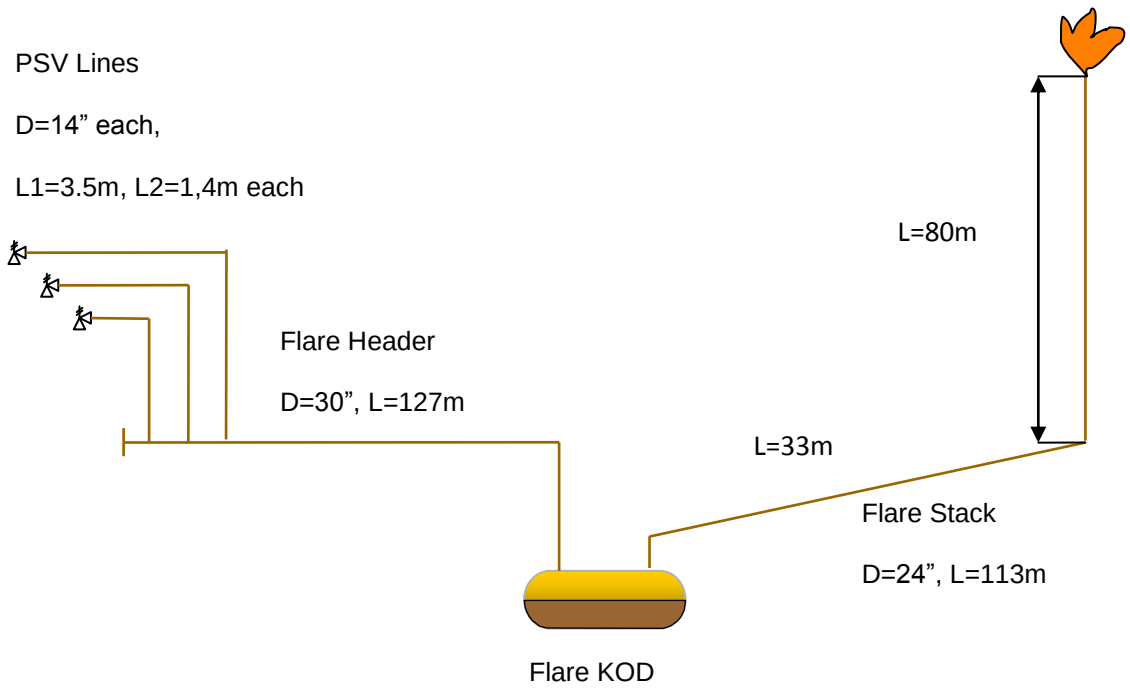

The pipe network includes three 14-inch PSV lines (tailpipes) connected to a 30-inch flare header through 90 deg tee joints. The flare header connects with the flare Knock-Out Drum

(KOD) with length L=10m and diameter D=3,4m. The KOD connects with a 24-inch flare stack, which connects with the flare tip.

Flare Tip

The flare tip diameter was set to the downstream diameter of the stack. The flare tip was tuned to match the pressure drop curve (table) below.

Flare Tip

Pressure Drop Curve

Ref. Temp (°C): 65,2
Molar Weight (g/mol): 23,25

Mass Flow (kg/h)	Static dP (bar)
0	0,000
25000	0,010
50000	0,024
75000	0,043
100000	0,071
125000	0,111
150000	0,163
175000	0,230
200000	0,310
225000	0,404
250000	0,511
300000	0,759
400000	1,336
500000	1,937
600000	2,520
700000	3,100
800000	3,700
850000	4,000

Flare Stack

The flare stack consists of five pipe segments of equal diameter (24”), with a total length of 113m. The stack is vertical from the flare tip through the first 80 meters and with a nearly horizontal inclination of about 9,5 deg down to the KOD. Pipe material is stainless steel.

Flare Header

The flare header consists of 11 pipe segments with a total length of 127 meters. Different segments have varying inclinations, with a dip angle. Pipe material is carbon steel.

Tailpipes

The tail pipes consist of 2 pipe segments with a total length of 4,9 meters. It starts with a 3,5 m long dipping segment from the PSV, at an inclination of 25 deg from the horizontal and a 1,4 m long vertical segment down to the flare header. Pipe material is carbon steel.

PSV

Source inlet temperature and pressure were defined. Inlet temperature at source = 50 C, inlet pressure at source plus 10% accumulation = 55 bara.

Assumptions made included; i) No heat transfer, ii) Atmospheric ambient conditions (T = 15C, p = 1 atm) iii) External medium is Air.

Tables showing a detailed description of the flare network pipe dimensions are included in the appendix (Appendix D).

4.1 Case definition based on fluid composition

To broaden the scope of the research, different fluid types are considered. Single component Nitrogen gas, and multi-component hydrocarbon (HC) gas. The reason for this was to see if fluid type and composition would influence observed differences in simulation results between FlareNet and OLGA.

4.2 Cases within FlareNet

Several cases where run in FlareNet for the single phase gas flow. From among the available pressure drop correlations for pipe flow, simulations runs were made for the following models and correlations:

1) Isothermal gas
2) Adiabatic gas
3) Beggs and Brill (homogeneous) model

Results were to be compared for flow rates from 2,5MSm3/D to 25MSm3/D.

A look at the available tee correlations, Miller's and Gardel's tee correlation was done. A similar analysis of results for different flow rates was done. Validation was to be done for the friction factor correlations available in FlareNet, Chen's and Round's correlations.

4.3 FlareNet and OLGA

For comparison with FlareNet, an identical model was built in OLGA. Simulation runs where to be done for the different fluid types, under similar conditions. A description of the OLGA model has been presented in section 3.

Below are some significant differences in the OLGA model approach:

1) The flare tip in OLGA was modelled as an orifice valve. The valve model is HYDROVALVE. The valve was meant to imitate the flare tip pressure drop curve. The valve table included C_V values ranging from 0 to a maximum value, corresponding to valve opening from 0 to 1. Below is the relationship between valve C_V and pressure drop across the valve, for a given flow rate. Taken from the OLGA manual

   $C_v = \frac{Q}{\sqrt{\frac{\Delta p}{G}}}$ where

   C_V – Valve sizing coefficient (gallons/min/psi^0.5)

   Q – Flow rate (gallons/min)

   Δp – Pressure drop across valve (psi)

   G – Specific gravity (-)

   The flare tip curve in OLGA was tuned to match results from FlareNet. This was achieved by adjusting the maximum C_V value until the pressure drop across the valve for the given flow rate corresponded with results for FlareNet.

2) There are no tee correlations available in OLGA. In OLGA pressure drop at tees was accounted for using additional loss coefficients. Additional pressure loss is given by the formula

   $\Delta p = \frac{1}{2} C \rho U^2$ where C is the additional loss coefficient.

   Values for C where taken according to recommendations in Crane [3].

3) The PSV is represented by a closed node with a source in OLGA. Inlet temperature, inlet pressure, and steady state flow rate are specified.

4.3.1 6-inch expander pipe between PSV and 14-inch tailpipe

Part of the aims of this project was to explore how the simulation tools would handle sonic/ near sonic flow. Adding a 6-inch diameter and 0,3 meter long pipe upstream the 14-inch tailpipe resulted in sonic flow within the 6-inch pipe section, for reasonable high flow rates. This enabled an analysis of the effect of sonic/near sonic on simulation results compared between OLGA and FlareNet. Simulation runs for this case were only done with the multi-component hydrocarbon (HC) gas. But the major result analysis was done for the case without the 6-inch pipe.

5 Simulation runs

5.1 Simulation runs and comparison within FlareNet

As mentioned earlier simulations were run for flow rates ranging from 2,5MSm3/D to 25MSm3/D. The possibility of setting up several scenario cases in one run in FLARENET made this task easier, as all flow rates could be analysed in one run for each case.

The dependence of other flow parameters like; pressure, temperature, pressure drop, on flow rate was monitored. Observations were well within expectations, as pressure, temperature and pressure drop increased with increasing flow rate.

Simulations runs were also made with different pressure drop models available in the software. The pressure drop models analysed are: Isothermal Gas, Adiabatic Gas, and Beggs & Brill. Our interest was in how close the results from these correlations would be, for different fluid types and conditions; and finding out the reasons for any obtained results according to theory. This we are hoping will give us a better understanding of how the software works, and what correlations would best suit different flow conditions, types and fluid type. The results obtained for the three pressure drop models were compared, with details below.

5.1.1 Results obtained for HC gas stream

The first sets of simulations were run for a hydrocarbon stream with the composition as given below:

Table 5.1.1 – HC gas composition

Component	Mole%
N2	1.4499
CO2	0.259
C1	83.031
C2	11.63
C3	3.129
i-C4	0.215
n-C4	0.239
i-C5	0.026
n-C5	0.017
C6	0.004

The stream has a critical point of 72 bara pressure and, -48 ^{o}C temperature. Given the system's operating conditions, this stream would remain purely gaseous throughout the pipe network (100% vapour phase). So we have single phase gas flow, which implies that the flow is compressible, and the appropriate equations of state have to be used for accurate results.

5.1.2 Comparing pressure drop models in FlareNet

Table 5.1.2 - Statistical analysis of results from different pressure drop models

	Parameter	**Pressure**	**Temperature**
	Standard Deviation	1,684645352	0,988311179
IsoG/ADG	***Correlation***	0,999936345	0,999935666
IsoG/B&B	***Correlation***	0,999991402	0,999991094

Table 5.1.2, Fig 5.1 and Fig 5.2 show statistical and graphical comparison of the temperature and pressure distribution across the flare network for the 3 pressure drop models at a relief rate of 25MSm3/D.

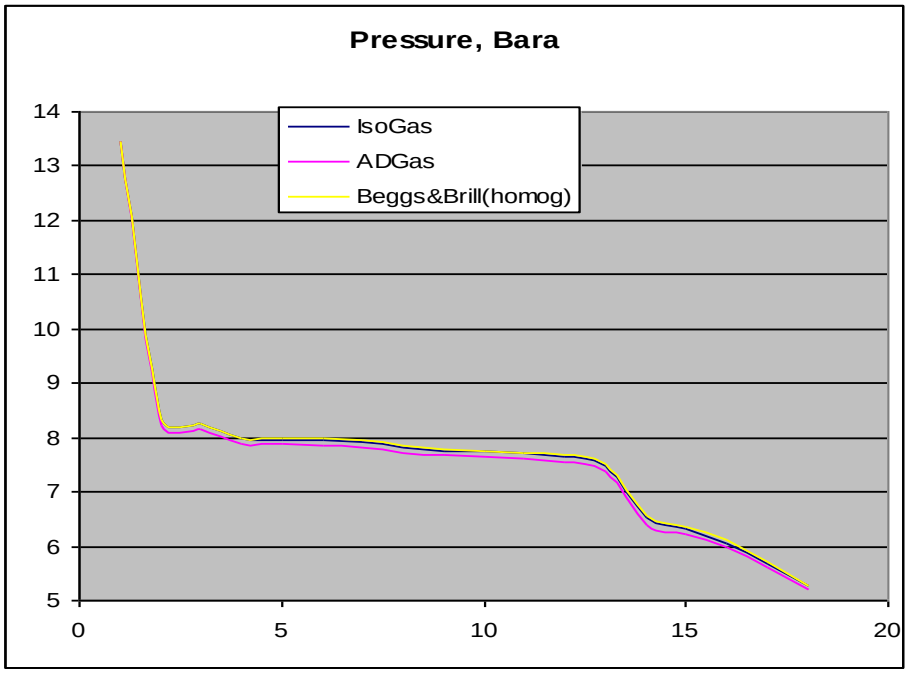

Fig 5.1 – System pressure profile calculated using the 3 different pressure drop models. X-axis represents positions starting from upstream tailpipe to upstream the flare tip. Y-axis shows pressure values.

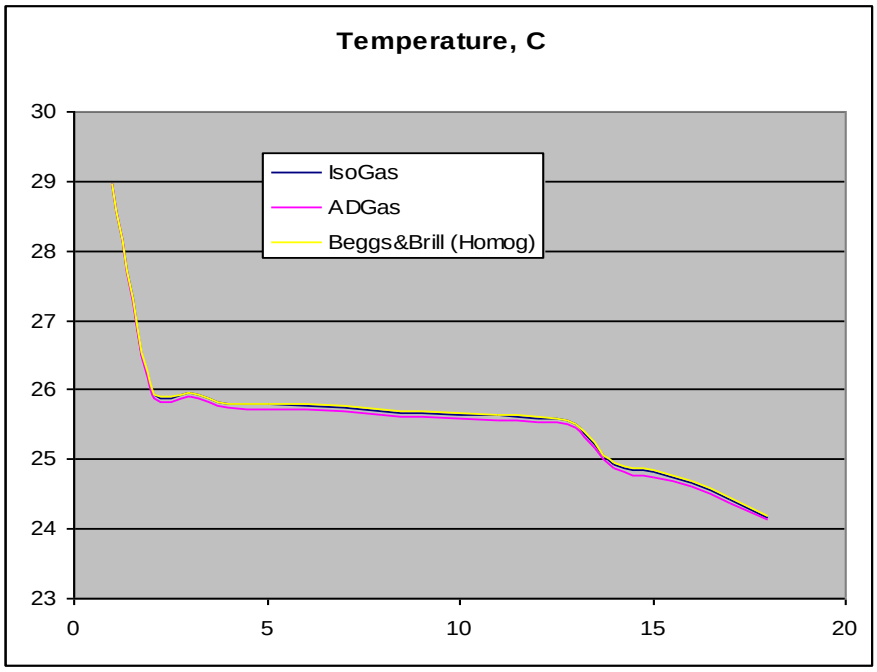

Fig 5.2 – System temperature profile calculated using the 3 different pressure drop models. X-axis represents positions starting from upstream tailpipe to upstream the flare tip. Y-axis shows temperature values.

From table 5.2, and as confirmed from the graphs, all 3 pressure drop models give very similar results for a purely gas stream, with very little variations. With correlation factors of 0.9999, when both the Beggs&Brill model and adiabatic gas were compared with isothermal gas it may be said that the all three models are acceptable; given that all other correlations and the equations of state are appropriately chosen.

As earlier noted in section 2, the recommended pressure drop correlation in FlareNet if the fluid is purely gas, is the Isothermal gas correlation. This is because Isothermal gas pressure drop model gives the best possible approximation for pressure drop in long gas pipeline systems. Adiabatic gas pressure drop model is usually recommended for systems with no heat lost or gained, short pipes with fast flow. And the Beggs&Brill (homogeneous) model is meant for multi-phase flow.

The trend remained the same for flow rates ranging from 2,5MSm3/D to 25MSm3/D. The possible reason for the nearly identical simulation results for pure gas flow could be the increased accuracy in calculations enabled by the option of splitting the pipes into smaller sections. This eliminates the effects from individual pressure drop models that are defined by the length of the pipe network. When used for single phase flow, multi-phase flow pressure drop correlations simplify to single flow equations.

It was interesting to see that the multi-phase pressure drop model (Beggs and Brill model) also gave acceptable results for a purely gaseous stream. Results where similar even for pipe segments with very high Mach numbers of 0,5 to 1.

5.1.3 Comparing Tee correlation models in FlareNet

The pressure drop across the tees is calculated using a number of tee correlations in FlareNet. Simulation runs where done for the Gardel correlation, and Miller's correlation. As noted earlier in section 2, the Gardel and Miller correlations are fits to experimental data carried out for different pipe diameters and flow rate intervals. So it was our aim to see how much they agreed under similar conditions. Runs where done for flow ranging from 2,5 to 25MSm3/D.

Below are plots and a statistical analysis of the results from both cases.

Table 5.1.3a – Pressure loss [bar] estimation with Miller's and Gardel's tee correlations

Q, MSm3/D	Miller		Gardel	
	Body	Branch	Body	Branch
2,5	1,245	1,242	1,246	1,238
5	1,796	1,785	1,798	1,777
7,5	2,513	2,494	2,516	2,481
10	3,305	2,279	3,309	2,262
12,5	4,115	4,082	4,12	4,061
15	4,935	4,895	4,941	4,87
17,5	5,752	5,706	5,759	5,676
20	6,566	6,514	6,574	6,48
22,5	7,377	7,318	7,386	7,28
25	8,196	8,131	8,207	8,088

Table 5.1.3b – correlation calculation for values estimated by Miller's and Gardel's tee correlations

	Body	Branch
Correl	1,00	1,00

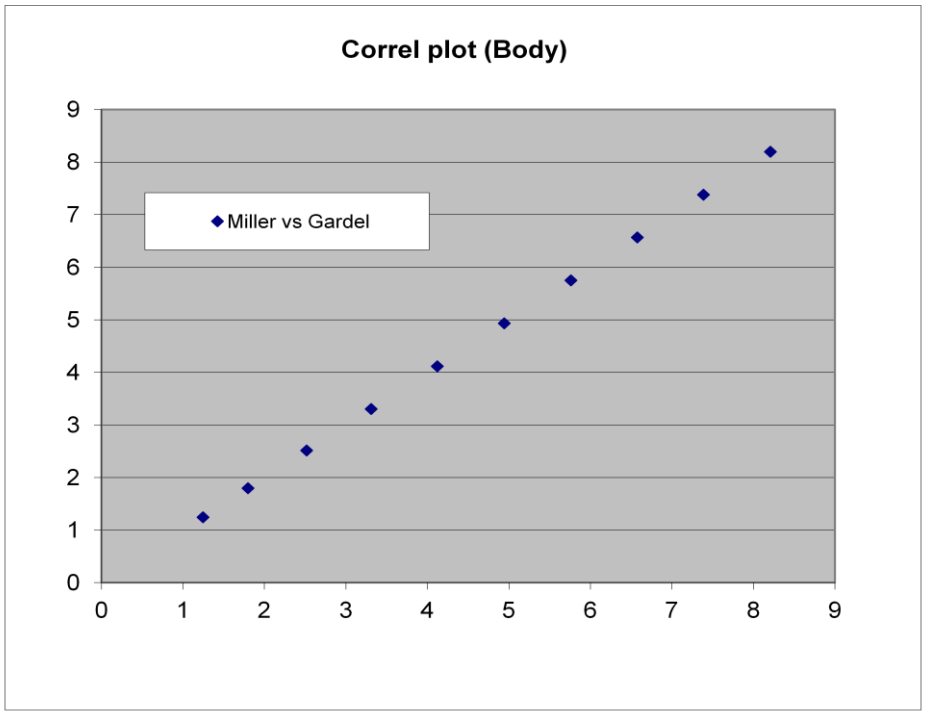

Fig 5.3 – Scatter diagram for estimated pressure upstream the Body of the tee joint

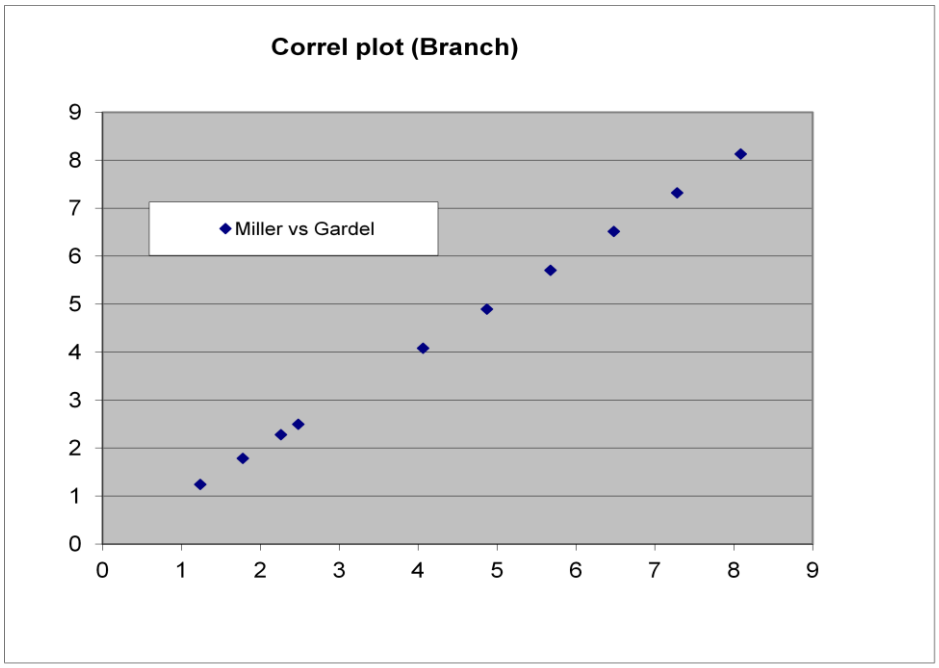

Fig 5.4 – Scatter diagram for estimated pressure upstream the Branch of the tee joint

The results correlated very well, with a correlation coefficient of 1.

5.1.4 Friction factor correlations

There are 2 main friction factor correlations available in FlareNet, Chen's friction factor correlation and Round's correlation. Both are explicit approximations of the Colebrook and White's implicit friction factor equation. Literature survey [7] showed that both are good approximations of the implicit version with little error, and are thus acceptable. The recommended correlation to use in FlareNet (by the vendor) is the Chen correlation, and it was used in all simulation runs done in FlareNet.

As a general benchmark, for highly turbulent flow (which is the case in a flare network) the friction factor is said to fall within the range of 0,015 [3]. Analysis of the friction factor values for all flow rates as obtained from FlareNet where within this range.

5.2 Cases for comparison between OLGA and FlareNet

In order to compare simulation results for FlareNet and OLGA, an identical model was built in OLGA. First for the multi-component gas flow case, PVT data was created using PVTsim20 and converted to an OLGA readable .tab file through the OLGA interface in PVTsim. Simulation runs where done for 10 flow rates split evenly between 2,5MSm3/D and 25MSm3/D.

A detailed analysis on the pressure and temperature change with varying flow rate was done.

In the earlier simulation runs for comparison of cases within FlareNet, there was little difference between the different pressure drop models available for single phase gas flow. The two models for gas flow looked at; Isothermal gas and adiabatic gas gave similar results. It was therefore decided to compare the results from just one of these models with the results from OLGA. The adiabatic gas pressure drop model, with Gardel's tee correlation model was picked. Friction factor correlation was Chen's correlation.

Energy balance

FlareNet has the option of including or excluding kinetic energy in the energy balance. For adiabatic flow

Energy balance with kinetic energy inclusion

$h + U^2/2 = \text{constant}$

Energy balance with kinetic energy exclusion

$h = \text{constant}$, where: h is the fluid enthalpy, and U is fluid velocity.

Runs were made for both cases in FlareNet, and it was observed that the inclusion of kinetic energy ($U^2/2$) in the energy balance had no effect on the pressure profile across the flare network, when compared with the runs excluding kinetic energy ($U^2/2$), for all flow rates.

There was a significant effect on the temperature though. The temperature change had an inverse relation to the flow speed (Mach number), across the flare network.

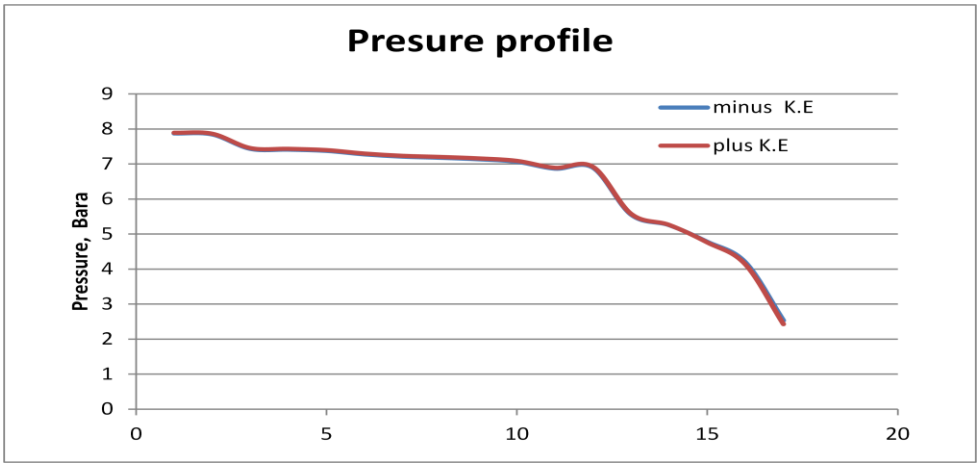

Fig 5. 5– Energy balance with/without K.E. for 25MSm3/D rate *

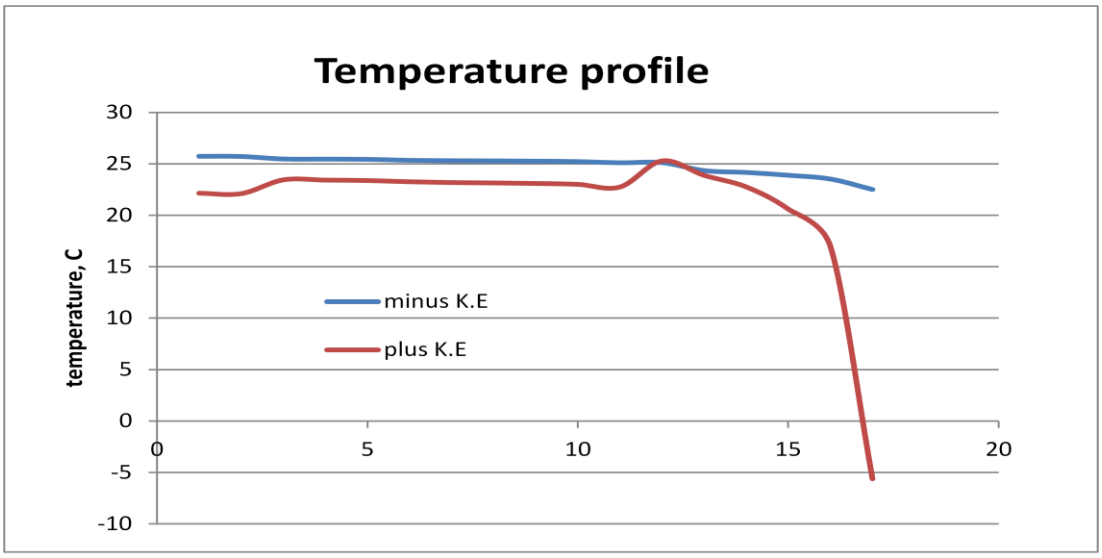

Fig 5. 6– Energy balance with/without K.E. for 25MSm3/D rate #

Comparing FlareNet runs with or without kinetic energy with OLGA, it was observed that the runs with kinetic energy inclusion in FlareNet gave similar temperature profiles with the OLGA runs. Therefore the decision was made to compare only FlareNet simulation runs with kinetic energy inclusion, with the OLGA runs.

**,# - x-axis represents positions from upstream the tailpipe to upstream the flare tip*

5.2.1 Case runs

5.2.1.1 Multi-component gas flow

With 6 inch (dummy) pipe from the PSV to tailpipe

A 6 inch (dummy) pipe was added between the PSV and 14 inch tailpipe, with a length of approximately 0,3 meters. Simulation runs where done in FlareNet and OLGA for flow rates mentioned above, ranging from 2,5 MSm3/D to 25MSm3/D. The flow was split equally among the 3 tailpipes (Q/3 in tailpipes).

General observations

It was observed that the system back pressure increased with an increase in flow-rate, both in OLGA and FlareNet. Flow speed within the 6 inch pipe was very high, reaching sonic values downstream for all flow rates. It was also observed that, as earlier stated (see energy balance above) the temperature profile across the network had an inverse relation to the flow speed/Mach number.

Figure 5.7 to 5.10 below show temperature and pressure profile plots of the flare network for FlareNet and OLGA, at flow rates of 2,5MSm3/D and 25MSm3/D. The profile starts from downstream the PSV to upstream the Flare tip.

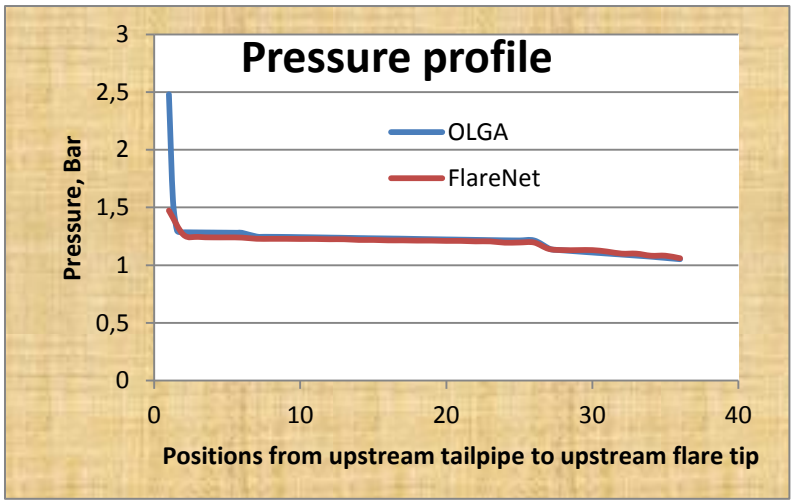

Fig 5.7 - System pressure profile for flow rate of 2,5MSm3/D

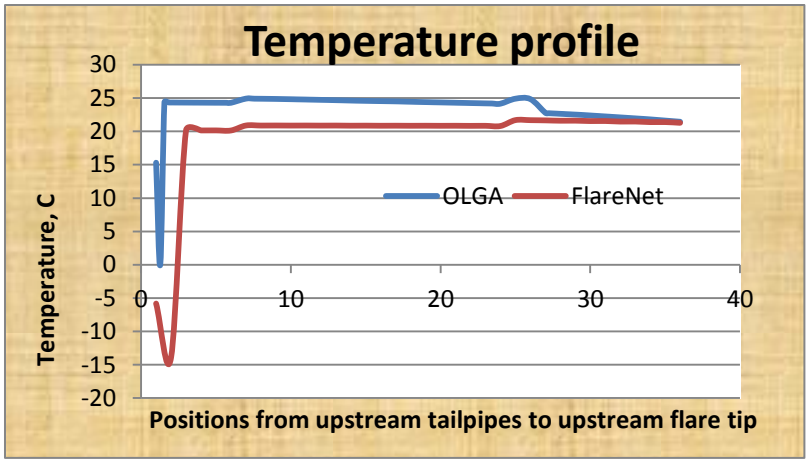

Fig 5.8 System temperature profile for flow rate of 2,5MSm3/D

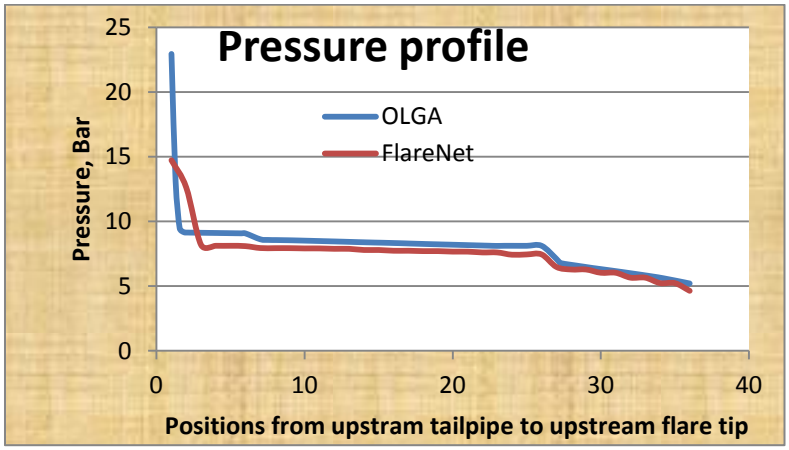

Fig 5.9 System pressure profile for flow rate of 25MSm3/D

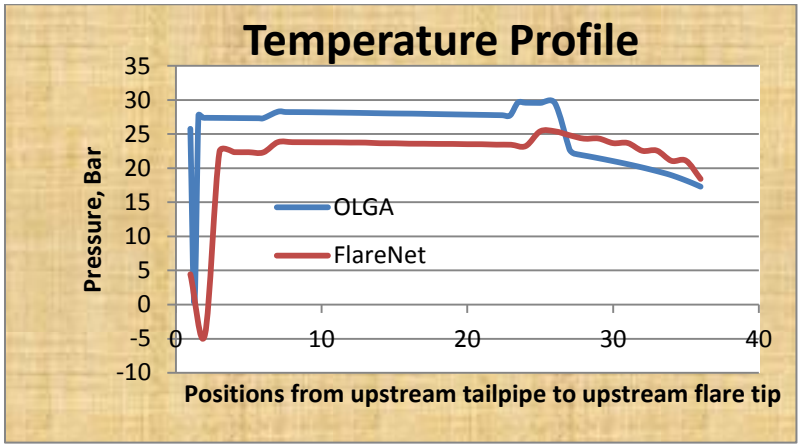

Fig 5.10 System temperature profile for flow rate of 25MSm3/D

Observations within FlareNet and OLGA compared

The flow velocities and Mach numbers for FlareNet and OLGA were comparably equal across the flare network. As expected, there was a huge pressure drop across the 6 inch pipe, where we have transition from sub-sonic to sonic flow both in FlareNet and OLGA. The

temperature drop was also considerably huge in both simulation tools. The drop in temperature may be explained from the energy balance equation. This agrees reasonably with theory.

The pressure and temperature profiles though, showed a difference in the estimated values across the flare network. As seen from figure 5.7 to 5.10 above, the estimated pressure and temperature values are comparably close upstream the Flare Tip, but drift wider apart down the network, with the maximum difference downstream the PSV.

Without 6 inch (dummy) pipe – tailpipe directly connected to the PSV

It was decided to run cases without the 6 inch pipe. Simulations were run for a new model, with the 6 inch pipe deleted. Flow rates were the same as for the previous case.

General observations

Observations for system back pressure were proportional to the flow rate, as was the system temperature. Flow velocities did not approach sonic values within the tail pipes.

Observations within FlareNet and OLGA compared

Flow velocities and Mach numbers were comparably equal for FlareNet and OLGA, across the flare network. Since the flow rates through the tailpipes were subsonic in this case, the pressure and temperature drops where not huge. They were within normal pressure drop limits and seemed to agree with theory.

As was observed for the case with 6 inch pipe included, the pressure and temperature in this case also showed a difference in estimated values. Observed differences in estimated values was most obvious upstream the tailpipe (downstream the PSV).

6. Results and Output

At this juncture, it will be good to restate the aims of this project. The aims/objectives of this project are:

1. Evaluate the simulation tools; FlareNet and OLGA and confirm if they operate according to already established theory based on which they were built. Things to be looked at included; the pressure drop models, friction factor correlations, and tee correlations in FlareNet.

2. Compare simulation results from FlareNet and OLGA, for flow in a simplified flare relief network under steady state conditions. Analyze the results to see if OLGA gives reliable estimates of the thermo-hydraulic parameters (P,T) under the high flow velocities encountered in flare systems, based on comparison with results from FlareNet.

Simulation output data for the system pressure, temperature, and velocity/Mach numbers were analysed and compared for the different cases.

A look at other system parameters such as mass, energy and momentum flux at branches with combining or dividing flow showed compliance with the conservation laws.

6.1 Multi-component gas case

Now we have a multi-component hydro-carbon gas with composition as seen in table 5.1.1. Simulation results for the different cases considered are presented below.

6.1.1 Case with 6 inch (dummy) pipe between PSV and Tailpipe

It is interesting to note that flow within the 6 inch pipe segment reached sonic values. The same observation was made for FlareNet and OLGA. This case gave us the opportunity to observe and analyze the flow behaviour under sonic conditions, as estimated by both simulation tools.

From the profile plots (Fig 5.7 to 5.8) the same flow behaviour across the flare network can be seen for both FlareNet and OLGA. Flow across the 6 inch pipe at sonic conditions lead to huge pressure and temperature drops. Temperature recovery (increase in temperature) for lower flow velocities within the 14 inch tailpipes, and 30 inch flare header is observed.

But upon comparing the output/results, the estimated thermo-hydraulic parameters (P,T) for FlareNet and OLGA varied across the flare network. In order to have a clear understanding of this behaviour a positional analysis of the flow parameters; pressure, temperature, and Mach number, was done. Plots of pressure, temperature and Mach number against flow-rate for different positions critical to flare system design were made.

Upstream Flare Tip

System pressure was taken in absolute values. The pressure upstream the Flare Tip equals the pressure drop across the Flare Tip plus atmospheric pressure.

In FlareNet the pressure drop across the Flare Tip was meant to match the flare tip pressure drop curve (see "Flare tip" in section 4).

In OLGA the Flare Tip was modelled as an orifice with a C_V tuned to match the pressure drop curve as in FlareNet (See details in section 4).

Below are the result plots of pressure, temperature, and Mach, against flow-rate, for FlareNet and OLGA at the Flare-Tip.

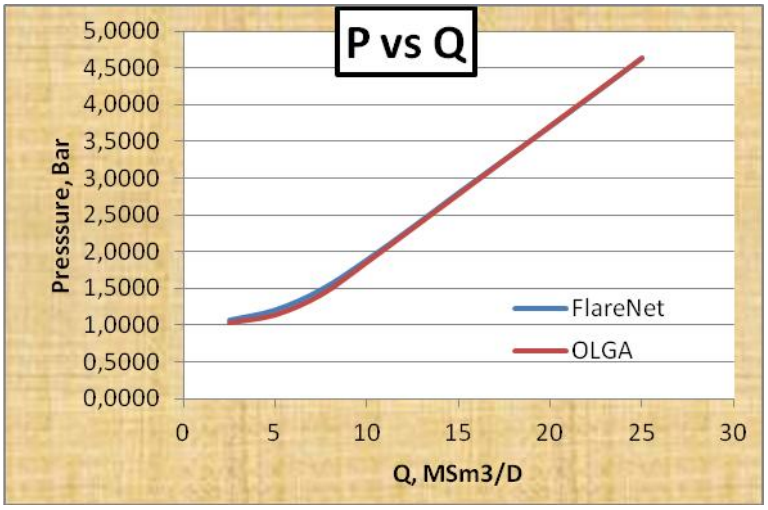

Fig. 6.1.1.1a – change of pressure with flow-rate at flare

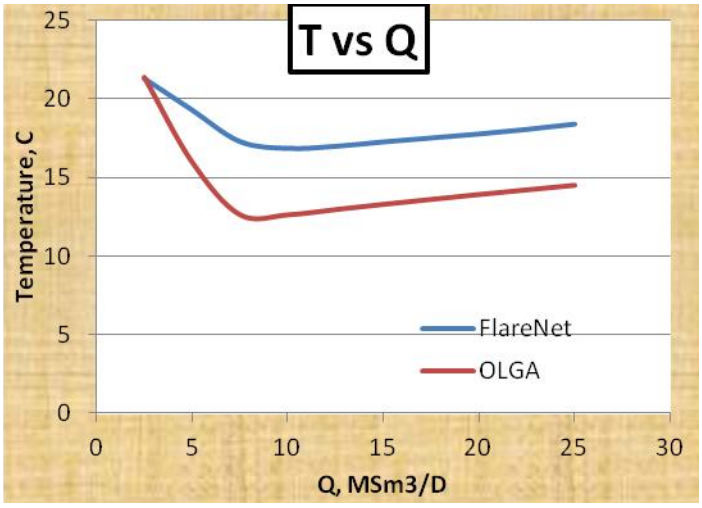

Fig. 6.1.1.1b – change of temperature with flow-rate at

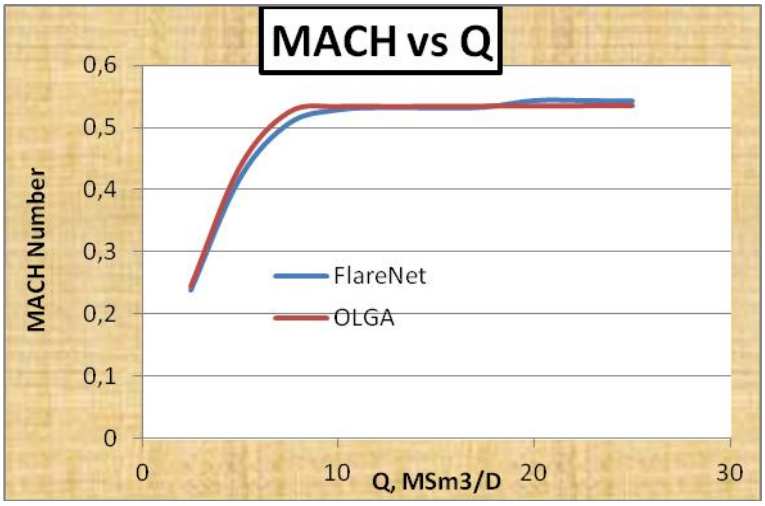

Fig. 6.1.1.1c – change of MACH with flow-rate at flare tip

Pressure and Mach match considerably well with little (negligible) difference between estimates by FlareNet and OLGA. Temperature shows a difference of about 3 degrees. OLGA shows a temperature estimate 3 degrees less that the FlareNet estimated temperature upstream the Flare Tip.

Upstream Flare Stack

Below are the result plots for pressure, temperature, and Mach, upstream the 20 inch Flare Stack.

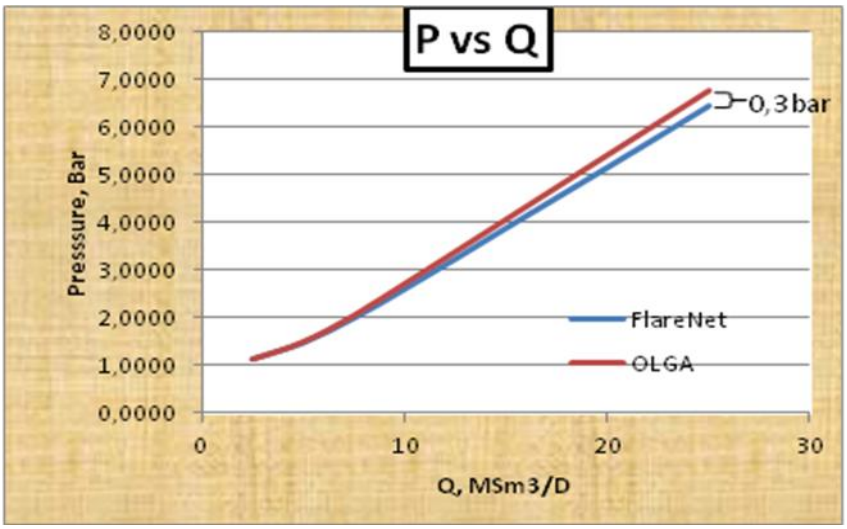

Fig. 6.1.1.2a – change of pressure with flow-rate at flare stack

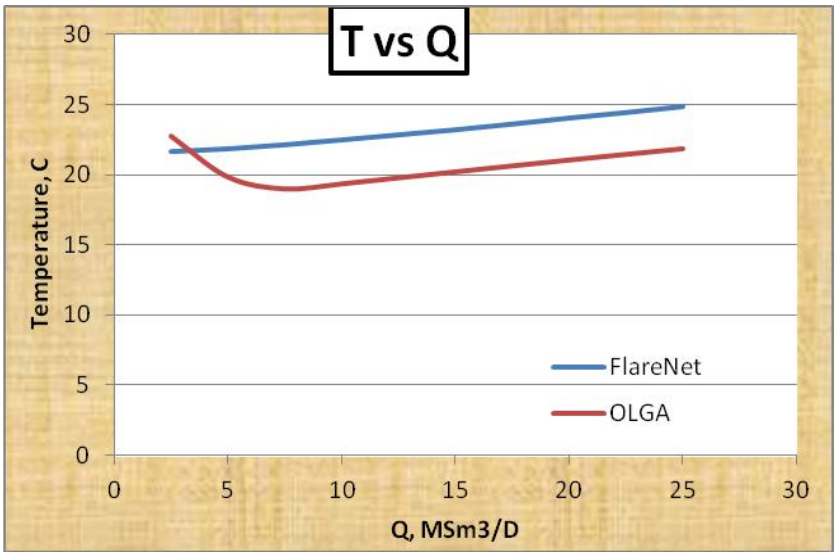

Fig. 6.1.1.2b – change of temperature with flow-rate at flare stack

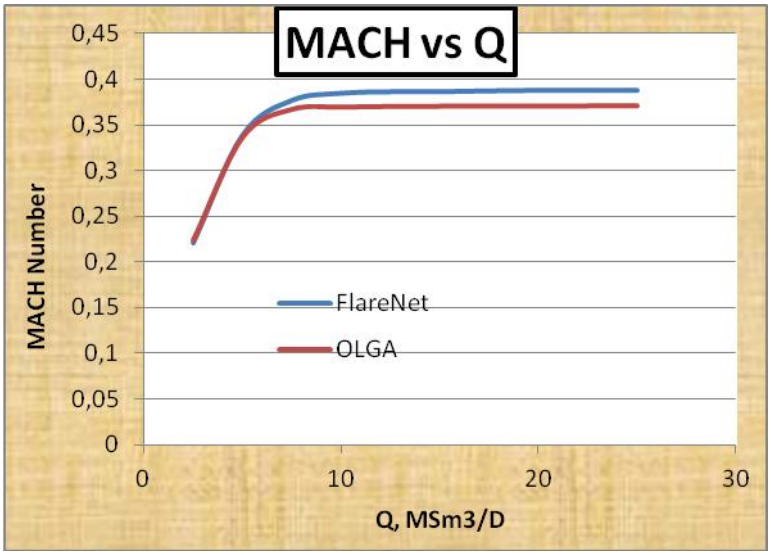

Fig. 6.1.1.2c – change of MACH with flow-rate at flare stack

Upstream the Flare Stack there is some noticeable difference in the estimated pressure and Mach number. OLGA shows a pressure estimate higher than that estimate by FlareNet by about 0,3 bar. The OLGA estimated temperature show a value about 3 degrees less than the FlareNet estimate temperature upstream the Flare Stack.

Inlet Knock-Out Drum

Figures 6.1.1.3(a,b,c) show the results at the inlet to the Knock-Out Drum (KOD).

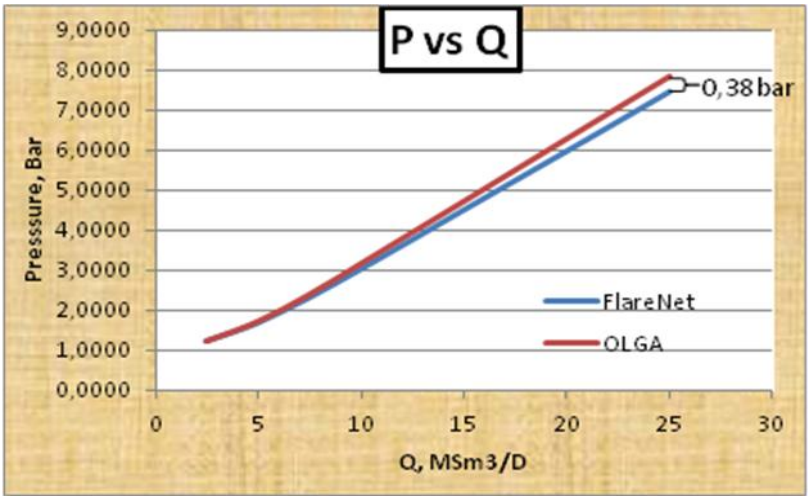

Fig. 6.1.1.3a – change of pressure with flow-rate at Knock-Out

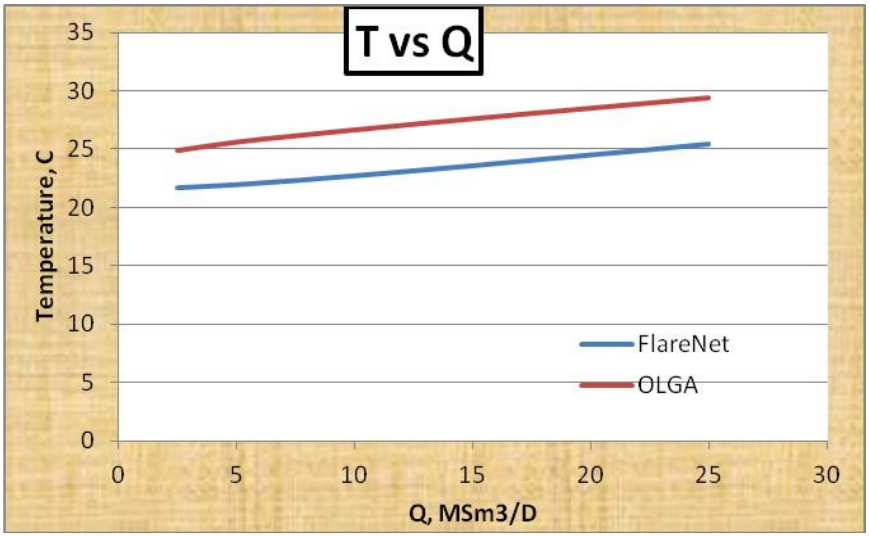

Fig. 6.1.1.3b – change of temperature with flow-rate at Knock-Out

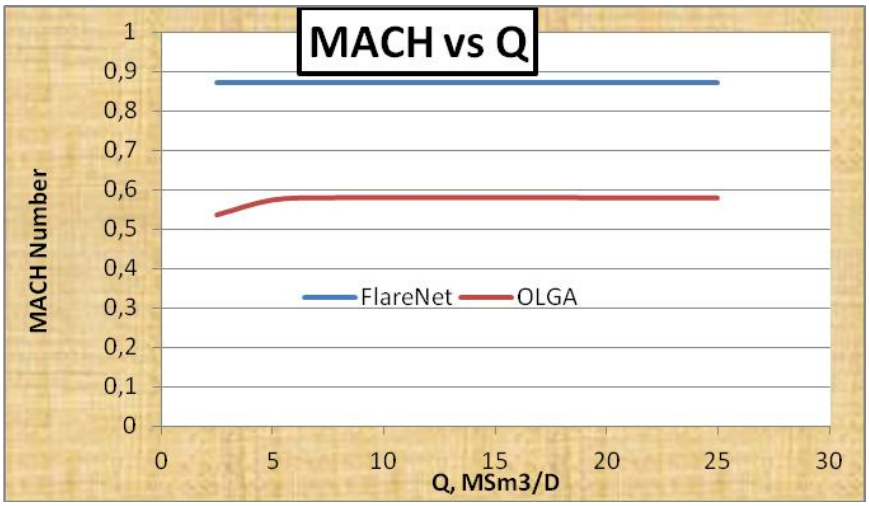

Fig. 6.1.1.3c – change of MACH with flow-rate at Knock-Out Drum

At the inlet to the Knock-Out Drum the difference in the estimated pressure has increased to about 0,38 bar, while the difference in the estimated temperature is about 3 degrees.

Upstream Flare Header (FH)

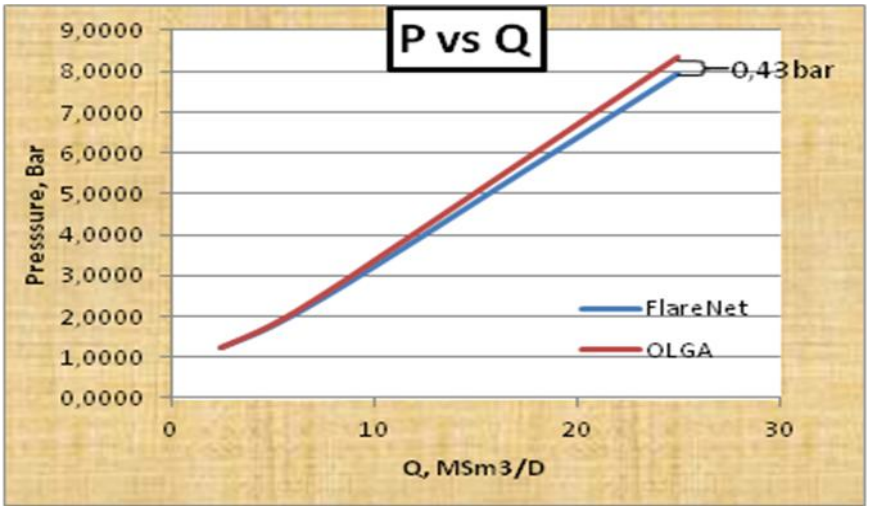

Fig. 6.1.1.4a – change of pressure with flow-rate at Flare Header

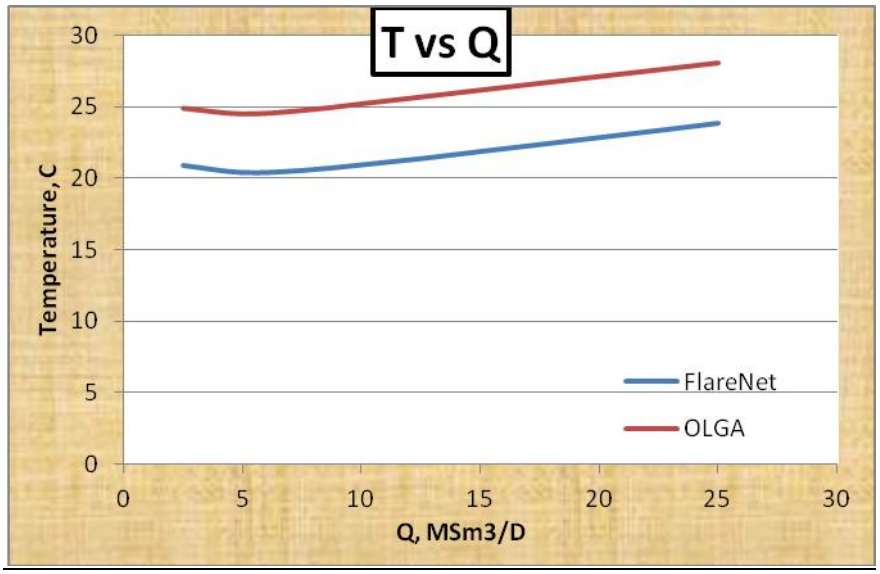

Fig. 6.1.1.4b – change of temperature with flow-rate at Flare Header

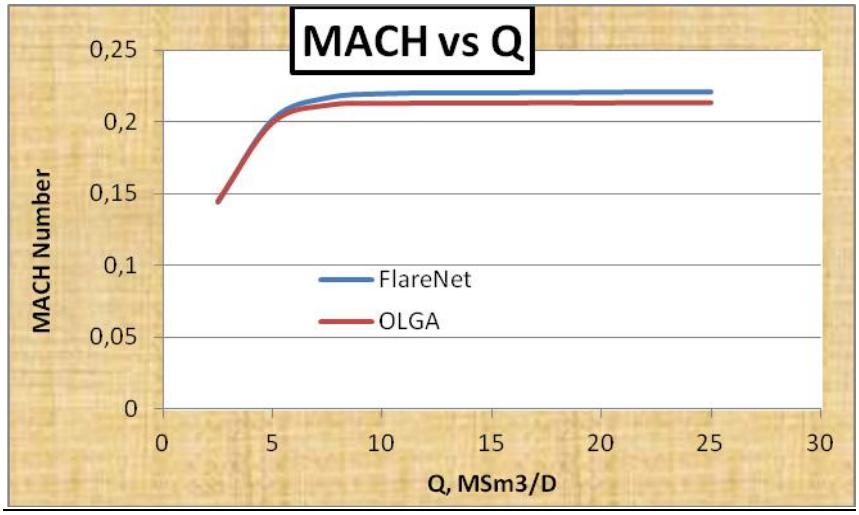

Fig. 6.1.1.4c – change of MACH with flow-rate at Flare Header

Upstream the Flare header the estimated pressure by OLGA exceeds that by FlareNet by about 0,43 bar. There is no significant difference in the estimated Mach numbers. OLGA shows a temperature estimate of about 5 degrees higher than that estimated by FlareNet.

Upstream 6 inch pipe (Downstream PSV)

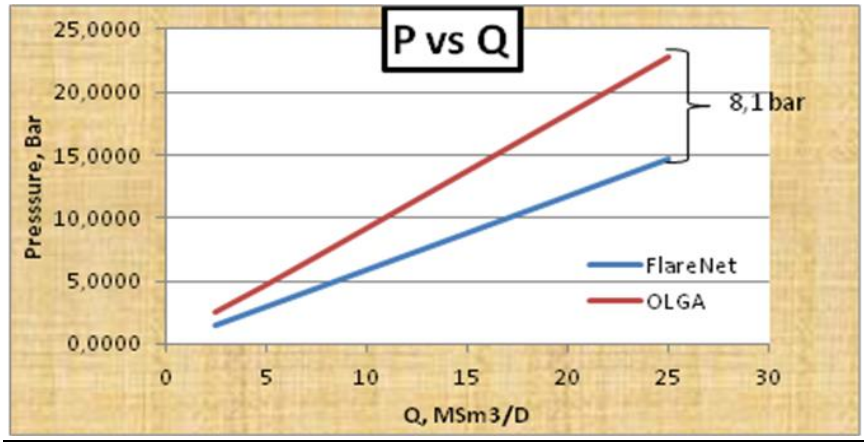

Fig. 6.1.1.5a – change of pressure with flow-rate downstream PSV

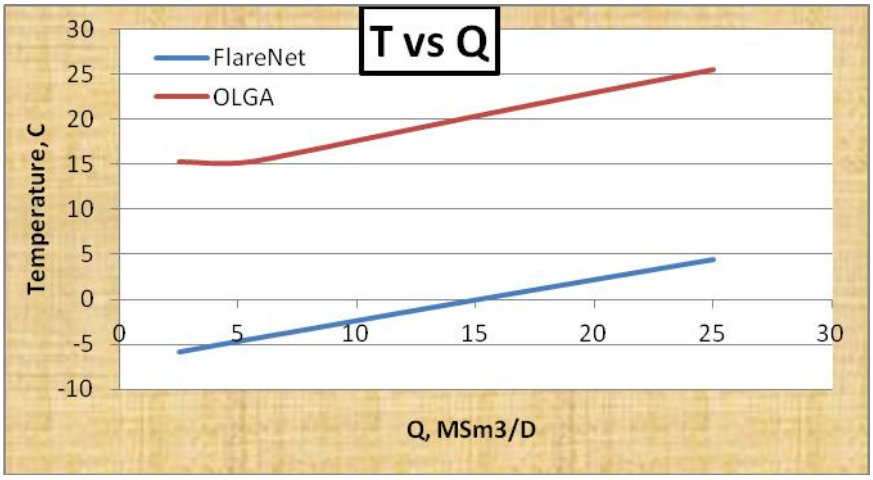

Fig. 6.1.1.5b – change of temperature with flow-rate downstream

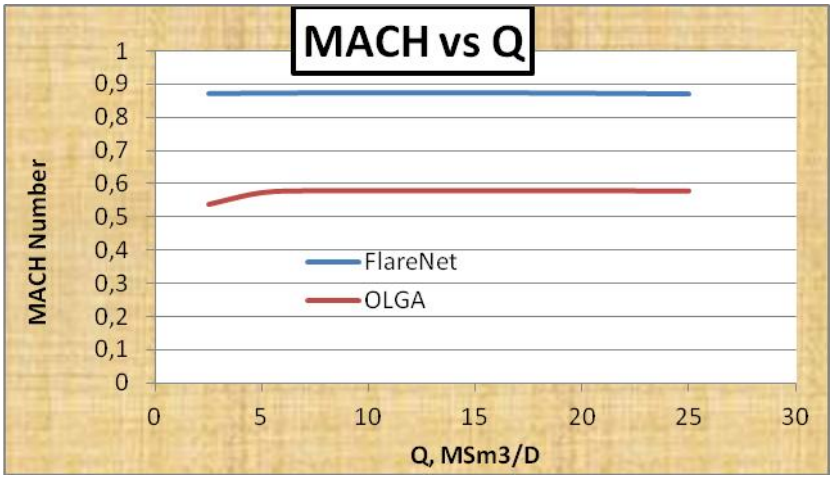

Fig. 6.1.1.5c – change of MACH with flow-rate at Flare Header

Downstream the PSV, OLGA shows an estimated pressure that exceeds the FlareNet estimated pressure by about 8,1 bar. The estimated temperature shown by OLGA also exceeds that estimated by FlareNet by about 20 degrees.

6.2.2 With 6 inch (dummy) pipe between PSV and Tailpipe deleted

For the case with the 6 inch pipe between the PSV and tailpipes deleted (the tailpipe directly connected to the PSV), the aim was to see how this change would affect the simulation results and how OLGA and FlareNet would compare. Some interesting observations were made, which will be looked at in the discussion.

FlareNet gave the same simulation results for each pipe segment as was for the case with the 6 inch pipe between the PSV and tailpipes. Only this time the pressure downstream the PSV equalled the pressure upstream the tailpipes. Position plots are presented below.

Upstream Flare Tip

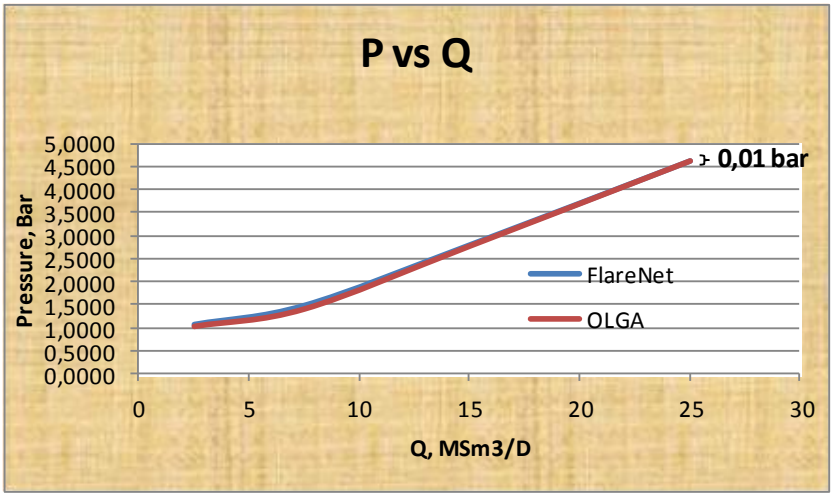

Fig. 6.1.2.1a – change of pressure with flow-rate at Flare Tip

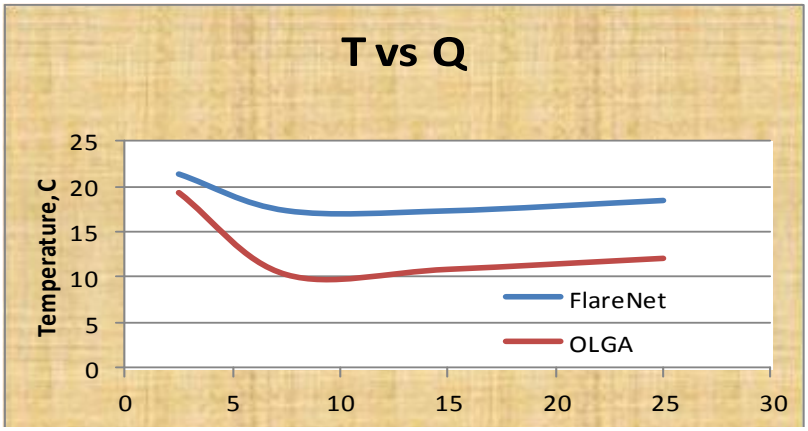

Fig. 6.1.2.1b – change of temperature with flow-rate at Flare Tip

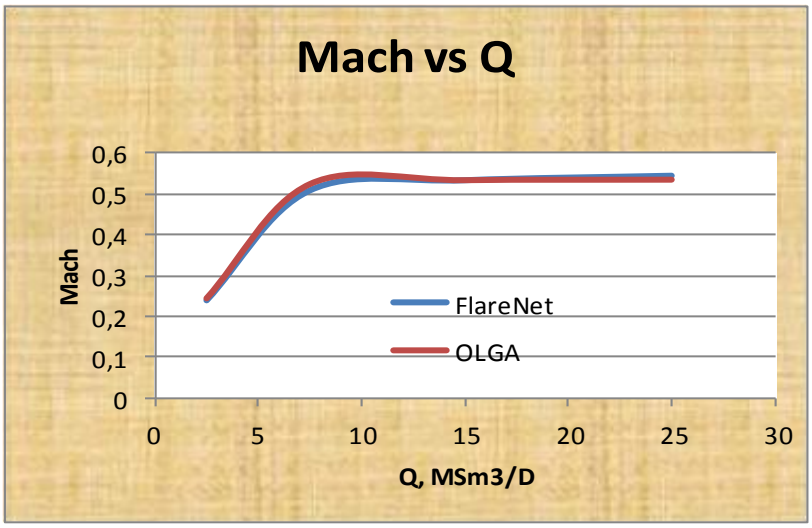

Fig. 6.1.2.1c – change of MACH with flow-rate at Flare Tip

Estimated pressure and Mach upstream the Flare Tip where approximately the same as the case with the 6 inch pipe between the PSV and the tailpipe. The estimated pressures and Mach numbers for both FlareNet and OLGA matched well for all flow rates. The estimated temperature shown in OLGA was as in the case with the 6 inch pipe, lower than the FlareNet estimate. The difference in estimated temperature hit a higher value of about 6 degrees.

Upstream Flare Stack

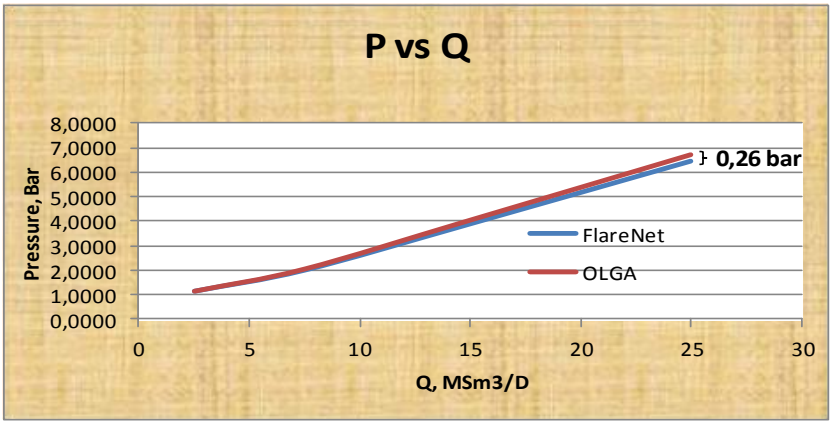

Fig. 6.1.2.2a – change of pressure with flow-rate at flare stack

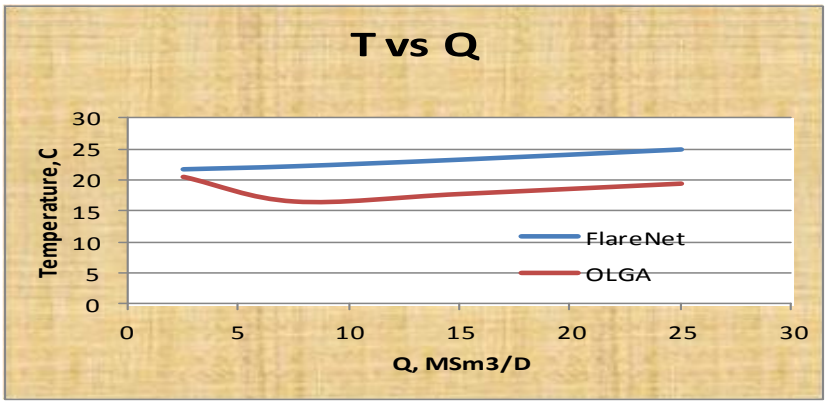

Fig. 6.1.2.2b – change of temperature with flow-rate at flare stack

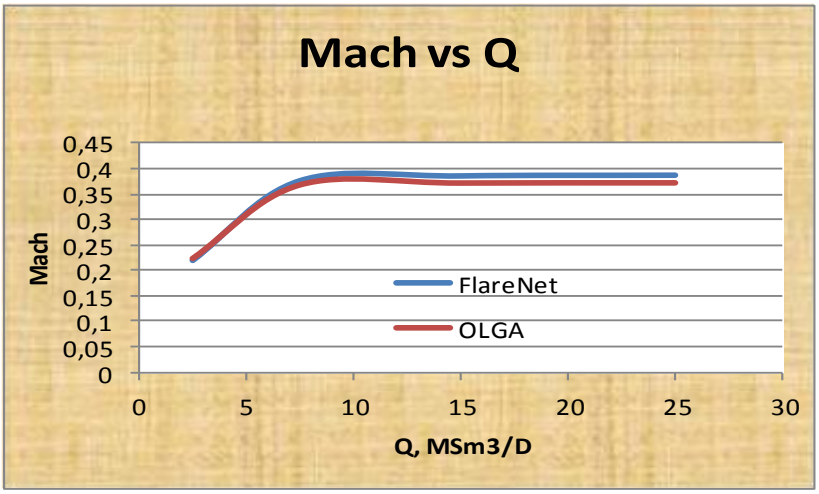

Fig. 6.1.2.2c – change of MACH with flow-rate at flare stack

Upstream the flare stack, the estimated pressures and Mach numbers matched reasonably well, but there are little difference which increased with increasing flow-rate. The difference in the pressure estimates reached a maximum value of about 0,26 bar at a flow-rate of 25MSm3/D. The difference in the temperature estimates had reduced to about 5 degrees.

Inlet Knock-Out Drum

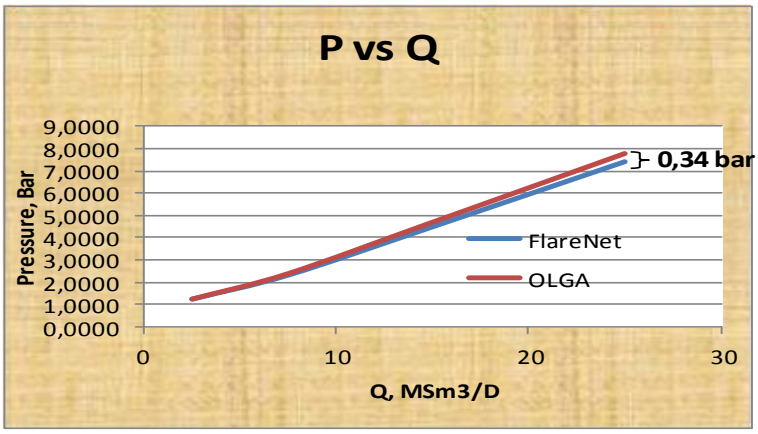

Fig. 6.1.2.3a – change of pressure with flow-rate Inlet of KOD

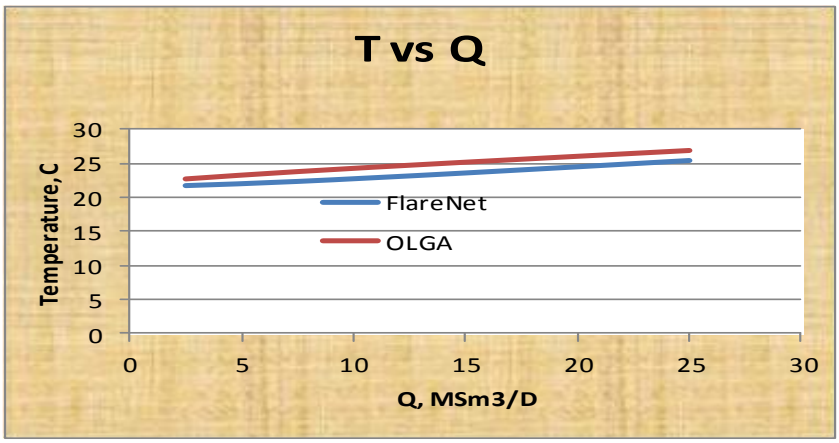

Fig. 6.1.2.3b – change of temperature with flow-rate Inlet of KOD

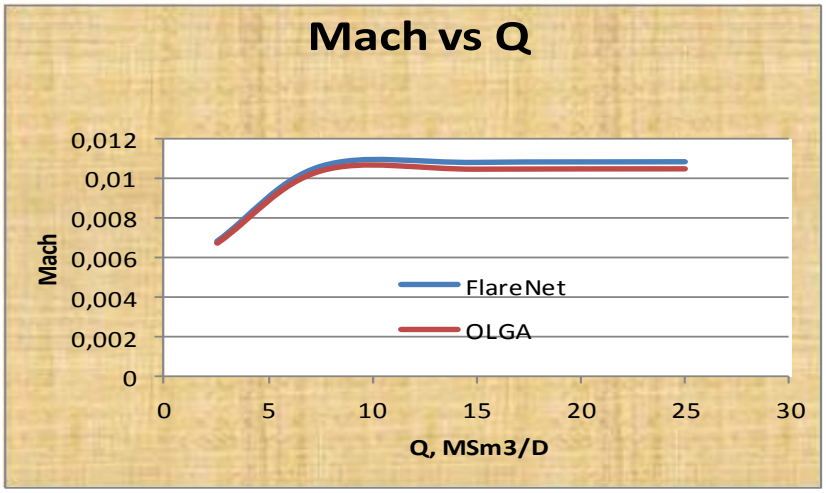

Fig. 6.1.2.3c – change of MACH with flow-rate Inlet of KOD

The pressure estimates at the inlet to the Knock-Out Drum followed the same pattern as upstream the flare stack. The difference in estimate pressure was about 0,34 bar, while that for the estimated temperatures had dropped to an absolute value of about 1 degree. The estimated temperature in OLGA has become higher than that in FlareNet.

Upstream Flare Header

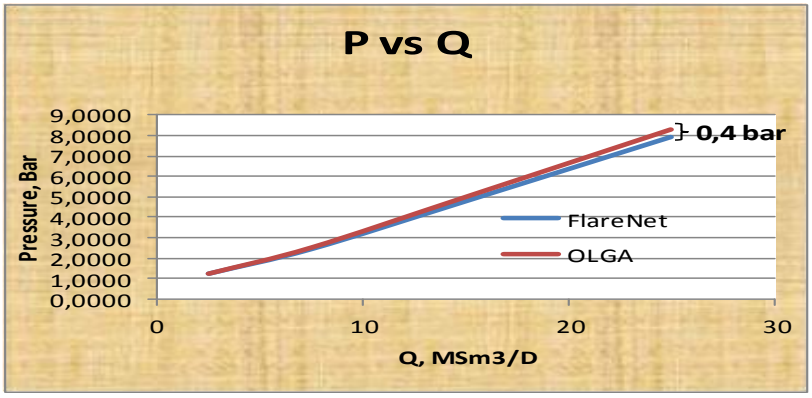

Fig. 6.1.2.4a – change of pressure with flow-rate at Flare Header

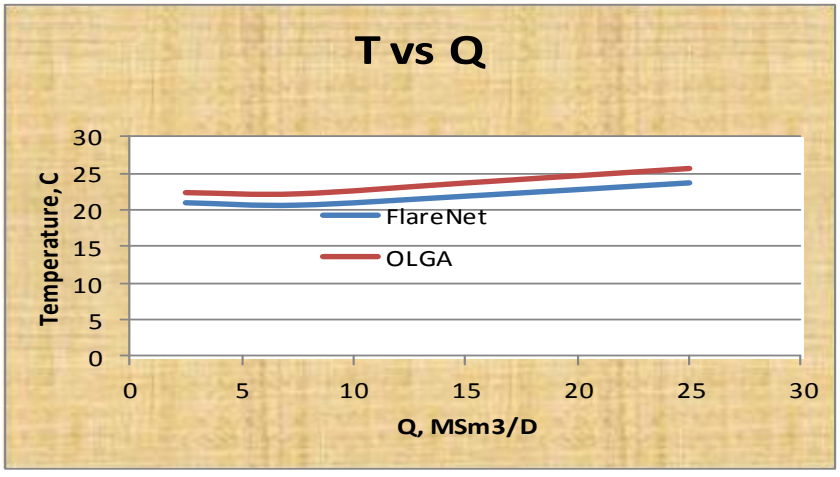

Fig. 6.1.2.4b – change of temperature with flow-rate at Flare Header

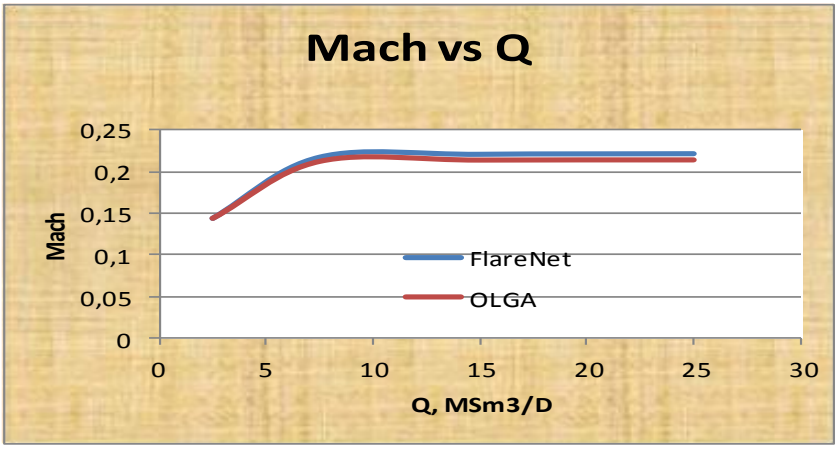

Fig. 6.1.2.4c – change of MACH with flow-rate at Flare Header

Upstream the Flare Header the difference in estimated pressures is about 0,4 bar, and that of the estimated temperature has increased to about 2 degrees.

Upstream Tailpipes (Downstream PSV)

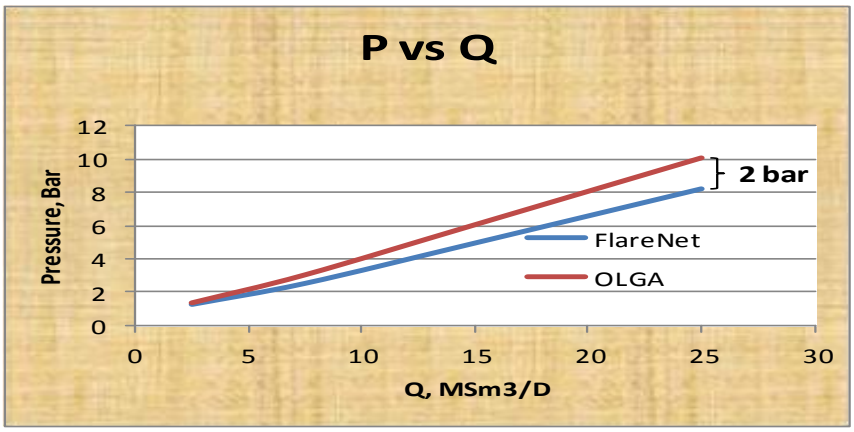

Fig. 6.1.2.5a – change of pressure with flow-rate downstream PSV

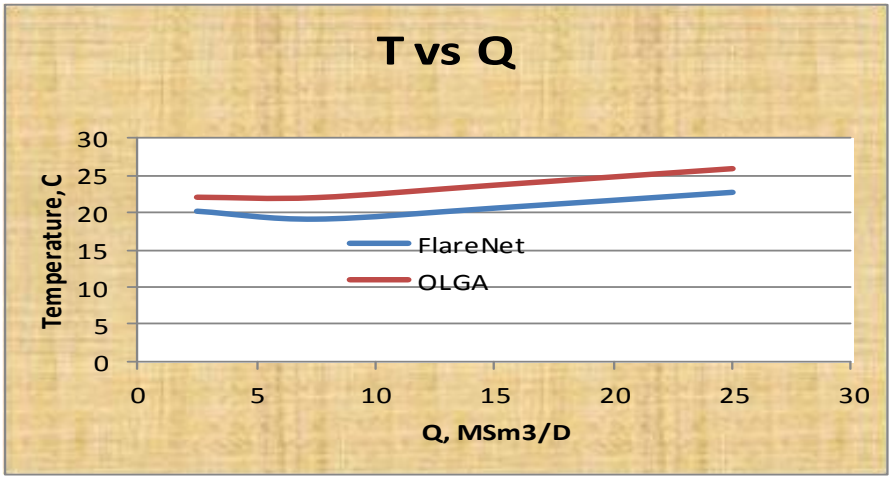

Fig. 6.1.2.5b – change of temperature with flow-rate downstream PSV

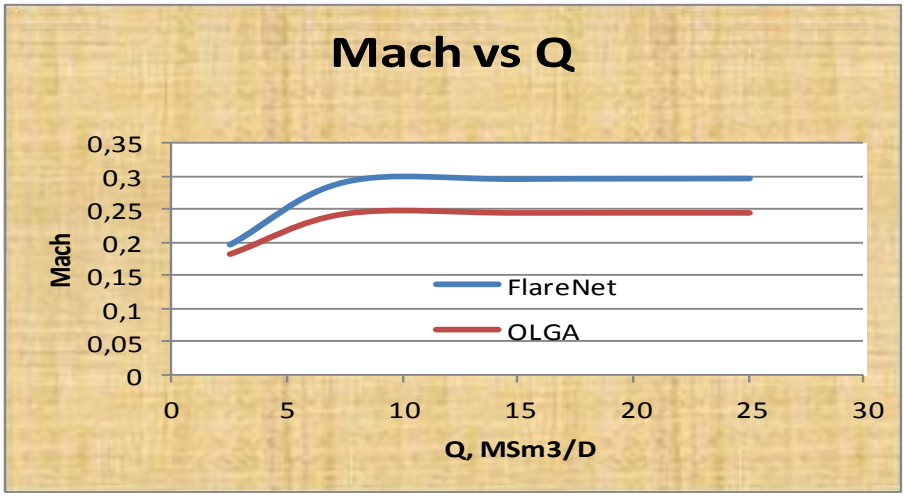

Fig. 6.1.2.5c – change of MACH with flow-rate downstream PSV

Downstream the PSV the difference in estimated pressure reaches a maximum value of about 2 bars at a flow-rate of 25MSm3/D. The difference in temperature and Mach numbers are about 3 degrees and 0,05.

Summary

For the multi-component hydrocarbon gas case, it was noticed that the pressure estimates at the flare tip are a good match, but there is some difference in the temperature estimates as shown by OLGA compared with FlareNet. The pressure and temperature increased with flow-rate, and down the flare network; from the flare tip to downstream the PSV.

Down the flare network there is a noticeable difference in the pressure estimated by OLGA, compared with FlareNet. This difference between the estimated pressures increases down the flare network and with increasing flow-rate. Reaching a maximum value downstream the PSV; at the highest flow-rate of 25MSm3/D.

The observed differences in estimated values reduced reasonably in the case with the 6 inch pipe between the PSV and tailpipe deleted, compared with the case that included it. The case with the 6 inch pipe included resulted in sonic flow downstream the 6 inch pipe. This gave very high pressure and temperature estimates in OLGA downstream the PSV. This translated to higher estimates across the flare network, than for the case with the 6 inch pipe deleted; for OLGA.

6.2 Nitrogen gas case

A case for pure nitrogen gas was looked at to see if gas composition had any significant effect on the observed differences in simulation results.

The simulation results showed a similar behaviour to the multi-component HC gas case. A pattern of increase in the differences in the estimated pressure by OLGA and FlareNet, from the flare tip down to the PSV tailpipes was observed. Observed differences for each position also increased with flow rate. Below are plots comparing results (Pressure and Mach) between OLGA and FlareNet.

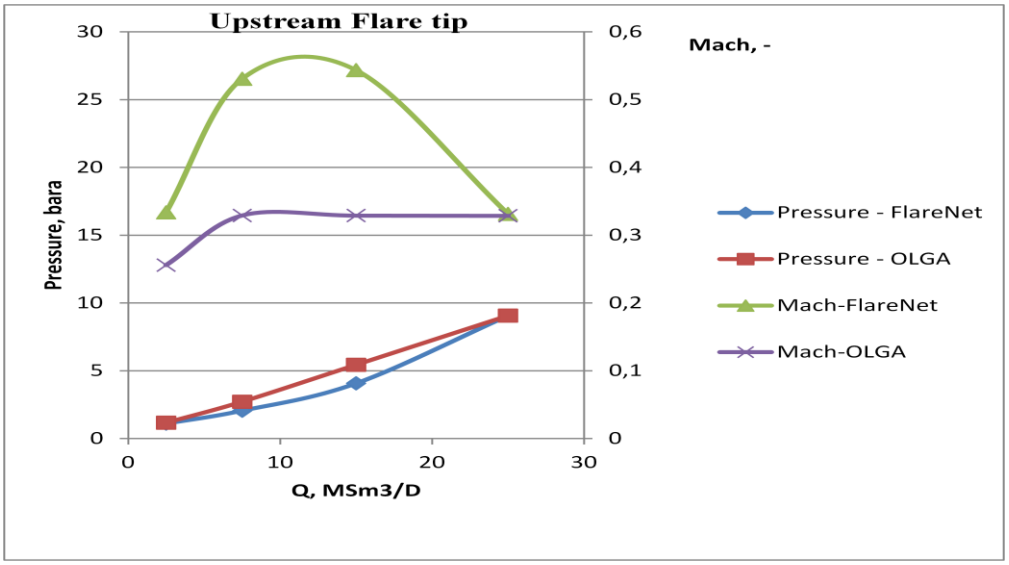

Fig 6.2.1 position plot for Nitrogen gas case upstream flare tip

As the results show, pressure was adjusted so that estimated values upstream the flare tip are approximately the same in OLGA and FlareNet. There seems to be some difference in Mach number for flow rates of 7,5 and 15 Msm3/D.

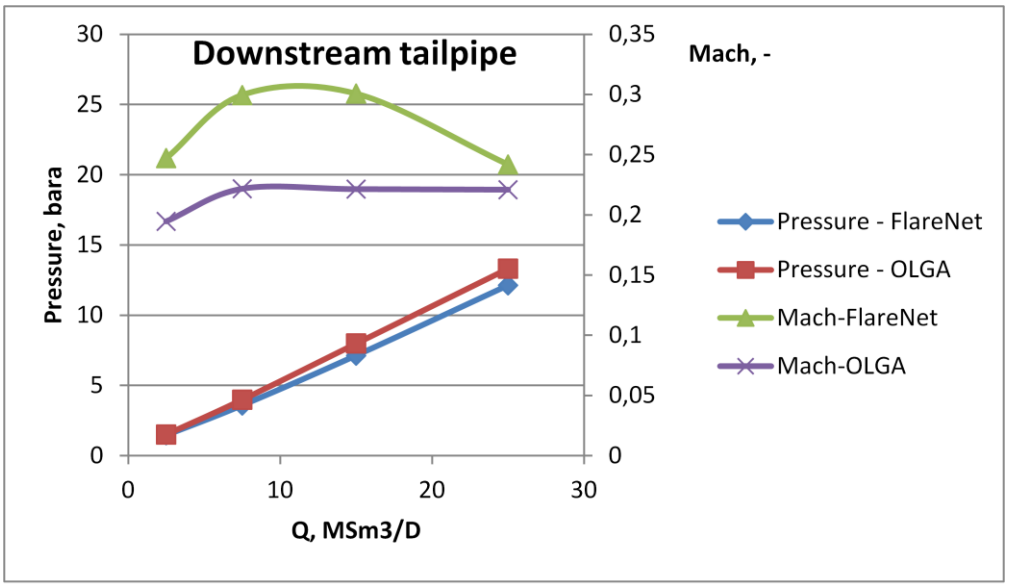

Fig 6.2.2 position plot for Nitrogen gas case downstream tailpipe

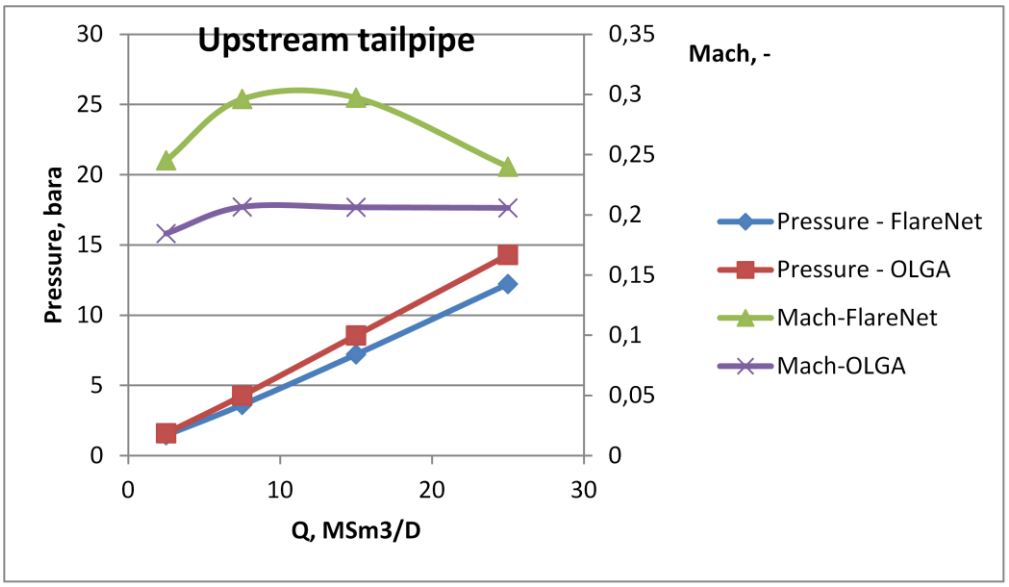

Fig 6.2.3 position plot for Nitrogen gas case upstream tailpipe

Plots were made to show how estimated pressure values changed from downstream to upstream the PSV tailpipes. The difference in estimated pressure upstream the tailpipe was approximately 2 bara at a flowrate of 25MSm3/D. We may recall that the same margin was observed for the multi-component HC gas case.

7.1 Within FlareNet

The simulation results in FlareNet using pressure drop calculation formulae for isothermal/adiabatic flow showed negligible variance in estimated results. It was therefore stated that for single phase gas flow, either pressure drop formula may be used. Simulation runs were done under the same initial conditions, with the assumption of no heat transfer. The Beggs and Brill multi-phase flow pressure drop correlation also gave similar results as the single phase gas flow models. It must be noted therefore that estimated results are reflective of assigned assumptions.

[1] Indicates that single phase gas flow for air under isothermal and adiabatic conditions gave approximately the same results for pressure drop in the range of $p_2/p_1 > 0{,}9$. Therefore adiabatic gas flow may be approximated to isothermal gas flow for pressure drops within this range without significant error in results. A similar suggestion criterion is given for approximating compressible flow to incompressible flow in fluid dynamics literature, i.e. [3].

Given the high flow rates and relatively short pipe lengths as seen in flare pipe networks, assuming adiabatic flow will be the closest in describing the flow for a flare network. Actual gas flow though is not strictly adiabatic or isothermal [1].

Friction factor correlations and tee correlations seem to lie within theoretical limits. Estimated friction factor values lie within the range for turbulent friction factor values suggested in literature, i.e. [3]. The formulae for Chen's friction factor given in the FlareNet user manual [6], as well as the tee correlation equations, agree with formulae found in literature [2, 3, 7].

Gardel's and Miller's tee pressure loss correlations available in FlareNet give reasonable agreeable results. Using either of these correlations in FlareNet for tee pressure loss calculations would make little difference.

7.2 Inclusion or exclusion of kinetic energy (K.E.) in the energy balance in FlareNet

For the case involving inclusion/exclusion of K.E. in the energy balance for the flowing fluid, it was observed that the pressure estimation was not affected by the K.E. of the fluid, but the temperature strongly depends on the K.E. of the fluid. This may be explained by the fact that for compressible gas flow, the energy of the fluid is represented solely by its enthalpy and K.E. According to [1, 2] under the assumptions of a perfect (ideal) gas, the enthalpy of the fluid is a function only of temperature. This leads to an energy balance equation of the form

$$c_p T_1 + \frac{U_1^2}{2} = c_p T_2 + \frac{U_2^2}{2} = c_p T_0 \qquad (7.1)$$

For adiabatic flow, and

$$\frac{U_1^2}{2} + q_H = \frac{U_2^2}{2} \qquad (7.2)$$

For isothermal flow

Here q_H is also a function of temperature.

It is recommended therefore to include K.E. when possible, as it gives a more correct estimate (of temperature). Depending on the design objectives accurate estimation of temperature may be critical to reliability of the design. For cases where accuracy of temperature estimation is not a requirement, K.E. may be excluded for ease of simulation. Bearing in mind that actual compressible gas flow is not strictly adiabatic or isothermal, it is impossible to tell exactly if the change in temperature with K.E. as observed from the simulations is a true reflection of the processes that transpire under real operating conditions.

Upon comparison with OLGA, inclusion of K.E. in the FlareNet model gave a similar flow characterization with that shown by OLGA.

7.3 Comparing results between FlareNet and OLGA

From the results and output it was noticed that the simulation results from OLGA showed some deviation from the results from FlareNet. The deviation seemed to follow 2 patterns:

1. Steady increases in the error between estimated pressure from the flare tip to downstream the PSV (see Figures in section 5, 6).
2. A steady increase in the error between simulated values with increasing flow rate for a given position (see section 6).

The variation in pressure and temperature as given in OLGA may be as a result of the following factors

- Error resulting from variable type in OLGA
- Error resulting from numerical procedures in OLGA

7.3.1 Error resulting from variable type

In section 3 it was stated that in FlareNet results for all variables are calculated for upstream and downstream positions of each pipe segment. OLGA classifies pipe section variables into two groups; boundary variables, and volume variables.

Boundary variables are computed at the section boundaries, while volume variables are computed at the middle of each section.

Pressure, temperature, and Mach number are volume variables. Velocity is a boundary variable. Results were compared based on upstream or downstream positions, to ensure similarity with FlareNet. This implies that the position results of pressure, temperature, and

Mach number from OLGA would not reflect exact values. Since the flow velocity changes very little within each section, this would have negligible effect on the Mach number. Estimated values of pressure and temperature though would be strongly affected, but the error can be minimized by breaking each pipe into small enough sections.

7.3.2 Error resulting from numerical procedures

The OLGA user manual version 7 states that pressure and temperature are de-coupled, meaning that current pressure (at section boundary N) is calculated based on previous temperature (at section boundary N+1). It further states that this de-coupling of temperature from pressure would normally give a wave propagation velocity in gas 15% too low. This would lead to some computational error.

Reference was also made in the OLGA user manual to flow speed. It is stated that due to the numerical solution scheme used in OLGA, it is particularly well suited for simulating rather slow mass flow transients. For fast transients, there are going to be numerical errors. It states that certain precautions with respect to spatial grid and time-stepping may be needed in order to keep the numerical error within acceptable limits.

7.4 Error analysis

7.4.1 Case with 6-inch pipe deleted

The OLGA estimated pressure values where higher than those of FlareNet. Assuming the FlareNet estimates to be correct, the error in estimated pressure by OLGA for the different flow rates for the case with the 6-inch pipe between PSV and tailpipes deleted is given in table 7.4.1a below.

From the table analyzing the results at each position, the error margin progressively increases with increasing flow rate. OLGA overestimates the pressure with a higher degree of error with increasing flow rate compared with FlareNet. Taking a look at the variation in results in terms of Mach number, no clear correlation could be established. Table 7.4.1b includes values of Mach numbers at the various flow rates. It appears that the Mach number remains approximately unchanged from flow rates of 7,5 to 25 MSm3/D (Mach and velocities are approximately equal for OLGA and FlareNet), at each position. But the error in estimated pressure progressively increased. This raises the question – how exactly does velocity contribute to the observed error? Mach numbers were within the range of <= 0,4. From the analysis above it may be said that for Mach numbers less than 0,4 error in estimated pressure by OLGA is for a function of the mass flux.

Table 7.4.1a – System pressure variation btw OLGA and FlareNet

		error	
Position	Q, MSm3/D	Pressure, %	ΔP error
Upstream tailpipe	2,5	9,42	0,117
	7,5	21,53	0,540
	15	23,14	1,140
	25	23,40	1,914
Upstream FH	2,5	0,66	0,008
	7,5	3,50	0,085
	15	4,75	0,227
	25	4,97	0,395
Inlet KOD	2,5	0,57	0,007
	7,5	3,07	0,070
	15	4,41	0,198
	25	4,60	0,342
Upstream Flare Stack	2,5	-0,58	-0,007
	7,5	1,98	0,040
	15	3,75	0,147
	25	4,00	0,259

Table 7.4.1b – Investigating role of Mach number in observed pressure variation

			error	
Position	Q, MSm3/D	Mach	Pressure, %	ΔP error,bara
Upstream tailpipe	2,5	0,198	9,42	0,117
	7,5	0,292	21,53	0,540
	15	0,297	23,14	1,140
	25	0,297	23,40	1,914
Upstream FH	2,5	0,144	0,66	0,008
	7,5	0,217	3,50	0,085
	15	0,221	4,75	0,227
	25	0,221	4,97	0,395
Inlet KOD	2,5	0,007	0,57	0,007
	7,5	0,011	3,07	0,070
	15	0,011	4,41	0,198
	25	0,011	4,60	0,342
Upstream Flare Stack	2,5	0,221	-0,58	-0,007
	7,5	0,377	1,98	0,040
	15	0,387	3,75	0,147
	25	0,388	4,00	0,259

7.4.2 Case with 6-inch pipe included

Given the analysis above that the error in estimated pressure by OLGA was not a direct function of velocity at Mach numbers below 0,4; it will be interesting to see how near sonic flow affects the simulation results. At sonic to near sonic flow pressure and temperature drops sharply (steeply), this was observed downstream the PSV. Estimated pressure and temperature are higher for equal flow rates, compared with the case without the 6-inch pipe.

Table 7.4.2a below shows details of error analysis downstream the PSV and upstream the flare header for case including 6-inch pipe.

Table 7.4.2a – Error analysis for sonic flow across 6-inch pipe

		FlareNet	OLGA	error	
Position	Q, MSm3/D	Mach	Mach	Pressure, %	ΔP error, bar
Downstream PSV	2,5	0,871	0,537	68,11	1,003
	7,5	0,872	0,578	55,78	2,463
	15	0,872	0,578	55,44	4,895
	25	0,871	0,577	55,12	8,113
Upstream Flareheader	2,5	0,144	0,145	0,79	0,010
	7,5	0,217	0,212	3,91	0,095
	15	0,221	0,213	5,22	0,249
	25	0,221	0,213	5,45	0,433

Compared with the case without the 6-inch pipe, the increase in Mach number (near sonic flow) seems to influence the resulting sharp increase in pressure drop both in OLGA and FlareNet, for equal flow rates. But again Mach number does not explain the progressive increase in estimation error for OLGA, with increasing flow rate. Even at near sonic flow, the increase in estimation error is not a direct function of Mach number.

7.5 More investigations

Taking a closer look at the results from section 6, a larger part of the variance in estimated pressure falls within the positions upstream the flare header to upstream the tailpipe. Here OLGA gives a pressure drop of about 1,76 bara while FlareNet gives 0,24 bara at a flow rate of 25MSm3/D for the case without 6-inch pipe. In previous work done by Kristian Nordberg (Aker Solutions MMO), which forms the basis for this work, a similar observation was made. More investigation has been done to figure out where this large difference comes from.

Table 7.5.1 below shows values of pressure and mach for different flow rates.

Table 7.5.1 – Analyzing pressure drop across the tee for FlareNet and OLGA

	FlareNet			OLGA	
Position	Q, MSm3/D	Pressure, bara	Mach	Pressure, bara	Mach
Upstream tailpipe	2,5	1,244	0,198	1,362	0,182
	7,5	2,509	0,292	3,049	0,243
	15	4,926	0,297	6,066	0,245
	25	8,180	0,297	10,095	0,245
Downstream tailpipe	2,5	1,238	0,199	1,296	0,191
	7,5	2,481	0,296	2,774	0,267
	15	4,869	0,300	5,515	0,269
	25	8,085	0,301	9,176	0,269
Upstream FH	2,5	1,228	0,144	1,236	0,144
	7,5	2,437	0,217	2,522	0,212
	15	4,780	0,221	5,007	0,213
	25	7,936	0,221	8,330	0,213
Downstream tailpipe pipe 1	2,5	1,240	0,199	1,298	0,191
	7,5	2,489	0,295	2,781	0,267
	15	4,886	0,299	5,528	0,268
	25	8,115	0,300	9,199	0,269

The highlighted numbers in table 7.5.1 show that pressure drop across the tee outlet/tail is about 0,15 bar in FlareNet, while in OLGA we have approximately 0,85 bar for flow rate of 25MSm3/D. This exceeds the value calculated with the tee correlation in FlareNet by 0,7 bar. Additional losses were added in OLGA to account for loss due to tees. Fig 7.5.1 shows the pressure drop from additional losses in OLGA

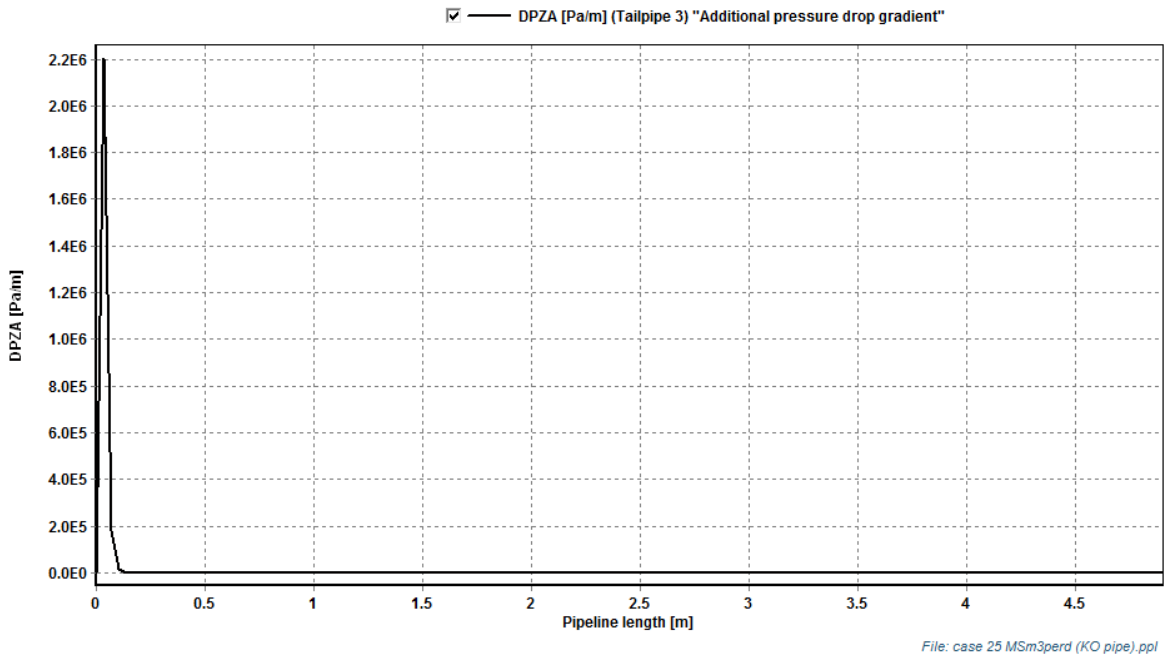

Fig 7.5.1 Additional pressure gradient from loss added upstream the internal node connecting tailpipe with flare header in OLGA to account for tee pressure loss calculations in FlareNet

DPZA (pa/m) approximately equals 2,2E06 was calculated over a section length of 0,028 m, and gives a pressure drop of approximately 0,6 bar. Comparing this value with the actual pressure drop across the node (0,85 bar), it may be said that the additional losses added in OLGA seem unnecessary. Inbuilt pressure drop calculations within the node seem to account for additional losses at the node (tee). Removing the additional losses would reduced the observed pressure drop from upstream the tailpipe to upstream the flare header in OLGA by 30%.

The analysis above puts the maximum pressure drop and highest contributor to the observed pressure drop across the tailpipe itself, at about 0,918 bar at 25MSm3/D flow rate. Further analysis was done to see the relationship between pressure drop and Mach number change in FlareNet and OLGA for all flow rates. Table 7.5.2 below shows the obtained values.

Table 7.5.2 – Pressure drop across tailpipe for different flow rates

Pressure drop across tailpipe			Change in Mach across taipipe	
	dp tailpipe, bar		dMach tailpipe, -	
Q, MSm3/D	FlareNet	OLGA	FlareNet	OLGA
2,5	0,006	0,066	0,00096	0,00917
7,5	0,028	0,275	0,00317	0,02378
15	0,057	0,552	0,00320	0,02435
25	0,095	0,918	0,00310	0,02438

Pressure drop and Mach number change across the tailpipe in OLGA is approximately 10 times more than the corresponding FlareNet values for all flow rates. The progressive increase in the difference in estimated pressure between OLGA and FlareNet seems to be connected with the change in Mach number across the pipe segment. OLGA having a higher variation in Mach number (a seemingly higher acceleration) across the segment gives a higher increase in pressure drop with flow rate.

Tables 7.5.3 and 7.5.4 show results from further analysis of the pressure drop and Mach within the tailpipe.

Table 7.5.3 – pressure and Mach number distribution within tailpipe for different flow rates

	FlareNet			OLGA	
Position	Q, MSm3/D	Pressure, bar	Mach	Pressure, bar	Mach
Upstream tailpipe pipe 1	2,5	1,244	0,198	1,362	0,182
	7,5	2,509	0,292	3,049	0,243
	15	4,926	0,297	6,066	0,245
	25	8,180	0,297	10,095	0,245
Downstream tailpipe pipe 1	2,5	1,240	0,199	1,298	0,191
	7,5	2,489	0,295	2,781	0,267
	15	4,886	0,299	5,528	0,268
	25	8,115	0,300	9,199	0,269
Downstream tailpipe pipe 2	2,5	1,238	0,199	1,296	0,191
	7,5	2,481	0,296	2,774	0,267
	15	4,869	0,300	5,515	0,269
	25	8,085	0,301	9,176	0,269

Table 7.5.4 - pressure drop analysis within tailpipe

Pressure drop and change of Mach number distribution within tailpipe					
		dp tailpipe, bar		dMach tailpipe, -	
Position	Q, MSm3/D	FlareNet	OLGA	FlareNet	OLGA
Tailpipe, pipe 1(inclined)	2,5	0,0043	0,0642	0,00068	0,00896
	7,5	0,0197	0,2679	0,00228	0,02315
	15	0,0401	0,5383	0,00238	0,02371
	25	0,0657	0,8963	0,00234	0,02373
Tailpipe, pipe 2 (vertical)	2,5	0,0017	0,0015	0,00028	0,00022
	7,5	0,0082	0,0067	0,00090	0,00063
	15	0,0171	0,0134	0,00082	0,00064
	25	0,0294	0,0222	0,00077	0,00064

The 14-inch tailpipe consists of 2 pipes, pipe 1 with L=3,5 and with an elevation of -1,5 (inclined) and pipe 2 with L=1,4 with an elevation of -1,4 (vertical). Comparing the pressure drop and change in Mach number in both pipes, it observed that the values are comparably equal for the vertical pipes. The huge difference in pressure drop is from the inclined upper

pipe directly connected to the PSV. It can also be observed that the pressure gradient within the tailpipe is constant for FlareNet, while OLGA shows a very huge variation between the two pipes.

Dukler's pressure drop calculation method breaks the pressure drop into its hydrostatic, frictional and acceleration components. In compressible gas flow, the hydrostatic pressure gradient is usually considered negligible and thus eliminated from most gas flow calculations. Fig 7.5.2 below shows the pressure gradient distribution within the tailpipe as estimated in OLGA.

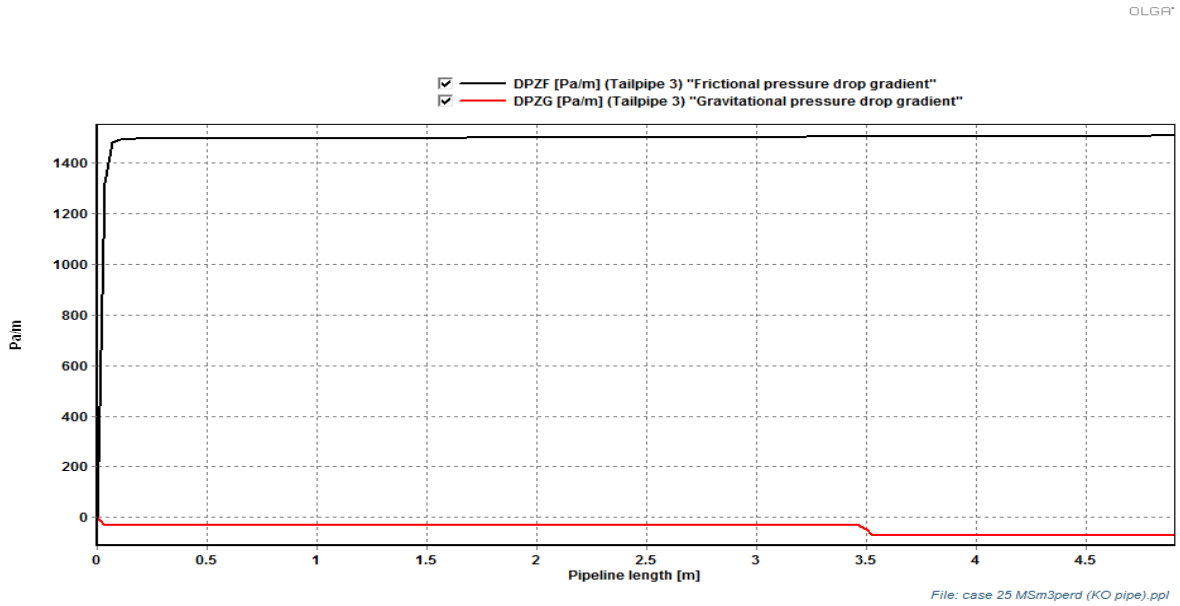

Fig. 7.5.2 Pressure gradient profile plot across tailpipe in OLGA, show the friction (black line) and gravity (red line) contributions. Vertical axis – pressure gradient [Pa/m], horizontal axis – pipeline length [m].

Fig 7.5.2 shows that that both frictional and gravitational pressure drop is calculated in OLGA. Frictional pressure gradient is approximately constant at a value of *1500* Pa/m corresponding to a frictional pressure drop of about **0,0735** bar across the tailpipe and about **0,021** bar across the vertical section of the tailpipe (14"). The contribution from gravity for the vertical section of the tailpipe is *-70* Pa/m, giving a pressure drop of **-0,00098** bar. The calculated frictional plus gravity pressure drop is comparably equal to values estimated from FlareNet. The observed difference in pressure drop across the tailpipe may thus be ascribed to acceleration effects in OLGA due to its higher variance in estimated flow velocity (Mach) across the pipe segment. This effect may equally be a reason for the observed differences in estimated pressure across the entire flare pipe network. True to general assumptions for gas flow, the contribution of gravity to the pressure gradient may be considered negligible.

Confirming the hypothesis

In order to get a clearer picture of the observed behavior within OLGA, a more detailed look was taken at the flow distribution within the inclined segment of the tailpipe (14”). The same investigation was carried out for the case with the 6” (dummy) pipe between the PSV and the 14” tailpipe; both within the 6” pipe and the inclined segment of the 14” pipe. Results are for a flow rate of 25MSm3/D. Tables 7.5.5 and 7.5.6 show the respective values.

Table 7.5.5 – Detailed investigation of flow within inclined segment of tailpipe, fully subsonic flow

Case without 6" (dummy) pipe (14" taipipe direct to PSV)									
Tailpipe, pipe1 in OLGA (14" inclined pipe)									
section #	length to mid-point, m	P , bara	dP, bar	T , °C	dT, °C	U, m/s	dU, m/s	Mach	dMach
1 (upstream tailpipe)	0,035	10,09480	0,772	25,962	0,823	0,000	98,662	0,245	-
2	0,070	9,32310	0,070	25,139	0,079	98,662	8,798	0,265	0,020
4	3,388	9,25330	0,055	25,060	0,061	107,460	0,695	0,267	0,002
100 (downstream pipe 1)	-	9,19850	-	25,000	-	108,155	-	0,269	0,002

Table 7.5.6 – Detailed investigation of flow within 6” and inclined pipe segments of tailpipe, sonic flow at expansion

Case with 6" (dummy) pipebetween 14" tailpipe and PSV									
Tailpipe, pipe1 in OLGA (6" (dummy) pipe)									
section #	length to mid-point, m	P , bara	dP, bar	T , °C	dT, °C	U, m/s	dU, m/s	Mach	dMach
1 (upstream tailpipe)	0,030	28,699	7,829	30,619	10,391	0,000	-	0,460	-
2	0,030	20,871	2,708	20,229	5,536	183,708	183,708	0,626	0,166
3	0,225	18,163	4,351	14,692	13,591	246,992	63,284	0,714	0,087
10 (downstream pipe 1)	-	13,812	-	1,101		345,983	98,991	0,916	0,202
Tailpipe, pipe2 in OLGA (14" inclined pipe)									
section #	length to mid-point, m	P , bara	dP, bar	T , °C	dT, °C	U, m/s	dU, m/s	Mach	dMach
1 (upstream pipe)	0,035	9,590	0,307	25,433	0,340	351,930	-	0,258	
2	3,395	9,283	0,084	25,094	0,094	103,816	-248,114	0,266	0,008
100 (downstream pipe 2)	-	9,198	-	24,999	-	108,155	4,339	0,269	0,002

Table 7.5.5 shows that in the case without the 6” (dummy) pipe, over 80% of the pressure drop across the inclined section of the tail pipe (0,77 out of 0,90 bar) is across the first section from the source (PSV). This is just over 1% of the pipe length. From figure 7.5.2, given that frictional pressure drop is nearly constant across the pipe section; this huge pressure drop across such a small pipe length must be due acceleration of the flow across that section. This effect may be because OLGA does not estimate (display) the velocity immediately downstream of the source, the source (PSV) in OLGA is placed at the middle of the section for which it is defined. Thus the flow velocity upstream of the section (upstream tailpipe), for which the source in OLGA is defined, is given as equal to zero (see Tables 7.5.5 and 7.5.6).

This would lead to a huge acceleration effect across that section from positions upstream to downstream.
This point is further emphasized upon analyzing the flow behavior across the 6" pipe and the inclined segment of the 14" tailpipe (for the case with the 6-inch (dummy) pipe included) – Table 7.5.6. Here the source is defined on section 1 of the 6" pipe, and the same behavior of pressure drop across the first section is exhibited. Well over 50% of the pressure drop across the 6" pipe falls across section 1 as well, and this may be associated with the rapid rise in velocity from 0 m/s upstream to about 184 m/s downstream that section. In this case pressure drop across section 1 of the 14" pipe falls well below its previous value (compare dP across section 1 for 14" pipe – Tables 7.5.5 and 7.5.6), even with an approximately higher velocity.

Assuming up-wind discretization of the velocity in OLGA i.e. velocity at the middle of a section equals velocity upstream that section. And given the Mach number range for the case without the 6" (dummy) pipe, flow may be approximated to incompressible flow. From Table 7.5.5 and fig 7.5.2, the frictional pressure drop across sections 2 to 4 approximately equals 1500*0,07 = **0,0105** bar. Using the formula for acceleration pressure drop for incompressible flow (see Appendix B), given: gas density = 7,3 kg/m^3 (as given in OLGA), U_1 = 98,66 m/s and U_2 = 107m/s, the acceleration pressure drop equals **0,0625** bar. This put the calculated pressure drop total pressure drop at **0,073** bar. The calculated value corresponds well that estimated from OLGA. Thus it can be said that the acceleration contribution to the pressure drop partly explains the difference in estimated pressure upstream the tailpipe for FlareNet and OLGA.

8 Conclusions

Difference in estimated pressure, Mach number and temperature between OLGA and FlareNet for the positions considered may be due to variable type. Pressure, Mach number and temperature are section variables, and are thus estimated as average/mid-point values for each section. Therefore displayed section values of these variables may not reflect the actual values for a give position, but this effect can be minimized by breaking pipe segments into small enough sections.
The de-coupling method used in the calculation procedures in OLGA may also lead to some error in estimated values by OLGA, though its effect was not determined in this work.

Including additional losses at the nodes to account for pressure loss calculations across tees as in FlareNet is unnecessary for OLGA. Pressure loss calculation in OLGA is inbuilt for nodes, and gives a roughly acceptable estimate.

The main reason for the observed difference in estimated pressure upstream the tailpipe is ascribed to acceleration effects in OLGA caused by a larger variation in estimated flow velocity (Mach) across first 2 sections of the tailpipe segment directly connected to the source, since frictional pressure drop calculated in OLGA is comparably equal to the pressure drop across the tailpipe as estimated from FlareNet.

It is recommended to split pipe segments that are connected to a source into small enough sections, and read off upstream values of estimated thermo-hydraulic parameters at about 2 section lengths from the source (section 3), in order to eliminate the pressure overestimation effect due to acceleration in OLGA (at high enough flow velocities). This may also be accomplished by including a dummy pipe of equal diameter and reasonable length between the source and the actual upstream pipe (in this case upstream the tailpipe), and reading off results at the inlet to the actual upstream pipe.

For steady state calculations like those performed in this work, given that OLGA and FlareNet perform calculations based on different thermodynamic packages, this may contribute to the observed difference in estimated thermo-hydraulic parameters. Given the pattern of increase in observed differences in estimated pressure from this work, such difference may increase for larger flare pipe networks, but they are also a function of the system Mach number.

Due to the high flow speed in flare networks, dynamic (transient) calculations with OLGA may give higher fluctuations from real-time operational values. But the observations from this work show that OLGA under steady state conditions reflects the same processes as FlareNet (see profiles and position plots of pressure, Mach, and temperature), and gives comparable estimates of pressure and Mach number. Therefore it may be concluded on this basis that OLGA will give realistic estimates if used for dynamic calculations for a flare network.

9 References

1. Fluid Mechanics with Engineering Applications; by Josheph B. Franzini, E. John Finnemore; Ninth Edition

2. Internal Fluid Flow: The Fluid Dynamics of Flow in Pipes and Ducts; by A. J. Ward-Smith (Jun 12, 1980)

3. Flow of Fluids Through Valves, Fittings and Pipe [Technical Paper No. 410]; by Crane Co. Staff (1985)

4. Two-phase flow in pipelines, course compendium; by Rune W. Time, UiS (2009)

5. OLGA user manual version 7, SPT group

6. Aspen Flare Systems Analyzer User Guide, Aspen Tech

7. Newly developed friction factor equation for pipe flow and flow assurance; by Ghanbari A., Farshad F. Fred and Rieke H. H., http://www.academicjournals.org/jcems, 2011

8. OTC 15186, Impact of Transient Analysis on Kuito Production Operations; by S. Song, Chevron Texaco E&P Technology Company; K. Peoples, Chevron Texaco Australia Pty. Ltd., 2003

9. Pressure-relieving and Depressuring Systems, API Standard 521, January 2007

10. Technical Safety, NORSOK Standard S-001, Edition 4, February 2008

11. Process Safety, NORSOK Standard P-100

12. Process Design, NORSOK Standard P-001

13. Flare Design Course: by Nelly Beate Terum, Senoir Engineer, Process, Aker Solutions; Bard Malstenbraten, Specialist Engineer, Process, Aker Solutions; December 2011

14. Flare Gas Systems Pocket Handbook; by K. Banerjee, N.P. Cheremisinoff, P.N. Cheremisinoff, 2003

15. Compressible Fluid Flow; by B.W. Imerie, Lecturer, Department of Engineering, University of Leeds

16. A Study of Two-Phase Flow in Inclined Pipes; by H. Dale Beggs, SPE-AIME, U. of Tulsa; James P. Brill, SPE-AIME, U. of Tulsa

Appendix A: Navier-Stokes equations in 3-D

Continuity Equation:

$$\frac{D\rho}{Dt} = \frac{\partial \rho}{\partial t} + \frac{\partial(\rho u)}{\partial x} + \frac{\partial(\rho v)}{\partial y} + \frac{\partial(\rho w)}{\partial z} = 0$$

It expresses the principle of conservation of matter. This is written for Cartesian coordinates x, y, z, measured relative to a stationary frame of reference, with corresponding velocity components u, v, and w.

Energy Equation:

$$\rho \frac{De}{Dt} = \frac{\partial}{\partial x}\left(k\frac{\partial T}{\partial x}\right) + \frac{\partial}{\partial y}\left(k\frac{\partial T}{\partial y}\right) + \frac{\partial}{\partial z}\left(k\frac{\partial T}{\partial z}\right) + \frac{p}{\rho}\frac{D\rho}{Dt} + \Phi$$

The equation may be written using enthalpy by substituting:

$$h = e + \frac{p}{\rho}$$

Giving $$\frac{Dh}{Dt} = \frac{De}{Dt} + \frac{1}{\rho}\frac{Dp}{Dt} - \frac{p}{\rho^2}\frac{D\rho}{Dt}$$

And substituting this we get

$$\rho \frac{Dh}{Dt} = \frac{Dp}{Dt} + \frac{\partial}{\partial x}\left(k\frac{\partial T}{\partial x}\right) + \frac{\partial}{\partial y}\left(k\frac{\partial T}{\partial y}\right) + \frac{\partial}{\partial z}\left(k\frac{\partial T}{\partial z}\right) + \Phi$$

Where Φ is the dissipation function.

Momentum Equation:

$$\rho \frac{Du}{Dt} = \rho X + \frac{\partial \sigma_{xx}}{\partial x} + \frac{\partial \tau_{xy}}{\partial y} + \frac{\partial \tau_{xz}}{\partial z}$$

$$\rho \frac{Dv}{Dt} = \rho Y + \frac{\partial \tau_{yx}}{\partial x} + \frac{\partial \sigma_{yy}}{\partial y} + \frac{\partial \tau_{yz}}{\partial z}$$

$$\rho \frac{Dw}{Dt} = \rho Z + \frac{\partial \tau_{zx}}{\partial x} + \frac{\partial \tau_{zy}}{\partial y} + \frac{\partial \sigma_{zz}}{\partial z}$$

Appendix B: Some important formulas

Chen's friction factor formula:

$$f_f = \left(-4log\left[\frac{\varepsilon}{3.7065} - \frac{5.0452}{R_e} log\left\{\frac{\varepsilon^{1.1098}}{2.8257} + \left(\frac{7.149}{R_e}\right)^{0.8981}\right\}\right]\right)^{-2}$$

Where:

f_f = Fanning friction factor

R_e = Reynolds number

ε = equivalent pipe roughness, ε = e/D = absolute pipe roughness/pipe internal diameter

Note: This is a turbulent friction factor. Flow in flare networks is considered turbulent.

Pressure drop from Dukler's method for single phase flow:

$$\Delta P_{total} = \Delta P_f + \Delta P_h + \Delta P_{acc}$$

$$\Delta P_f = \frac{2 f_f \rho u^2 L}{g D}$$

$$\Delta P_h = \rho g \Delta Z$$

$$\Delta P_{acc} = \frac{\rho}{2g}(u_2^2 - u_1^2)$$

Where:

ΔP_f = Frictional pressure drop

ΔP_h = Hydrostatic pressure drop

ΔP_{acc} = Acceleration pressure drop

and

ρ = fluid density (average value, for gas flow)

u = fluid flow velocity

L= pipe length

g = gravitational constant

D = pipe inner diameter

ΔZ = elevation

Appendix C: Subsonic flow of compressible fluid in a constant area duct [1]

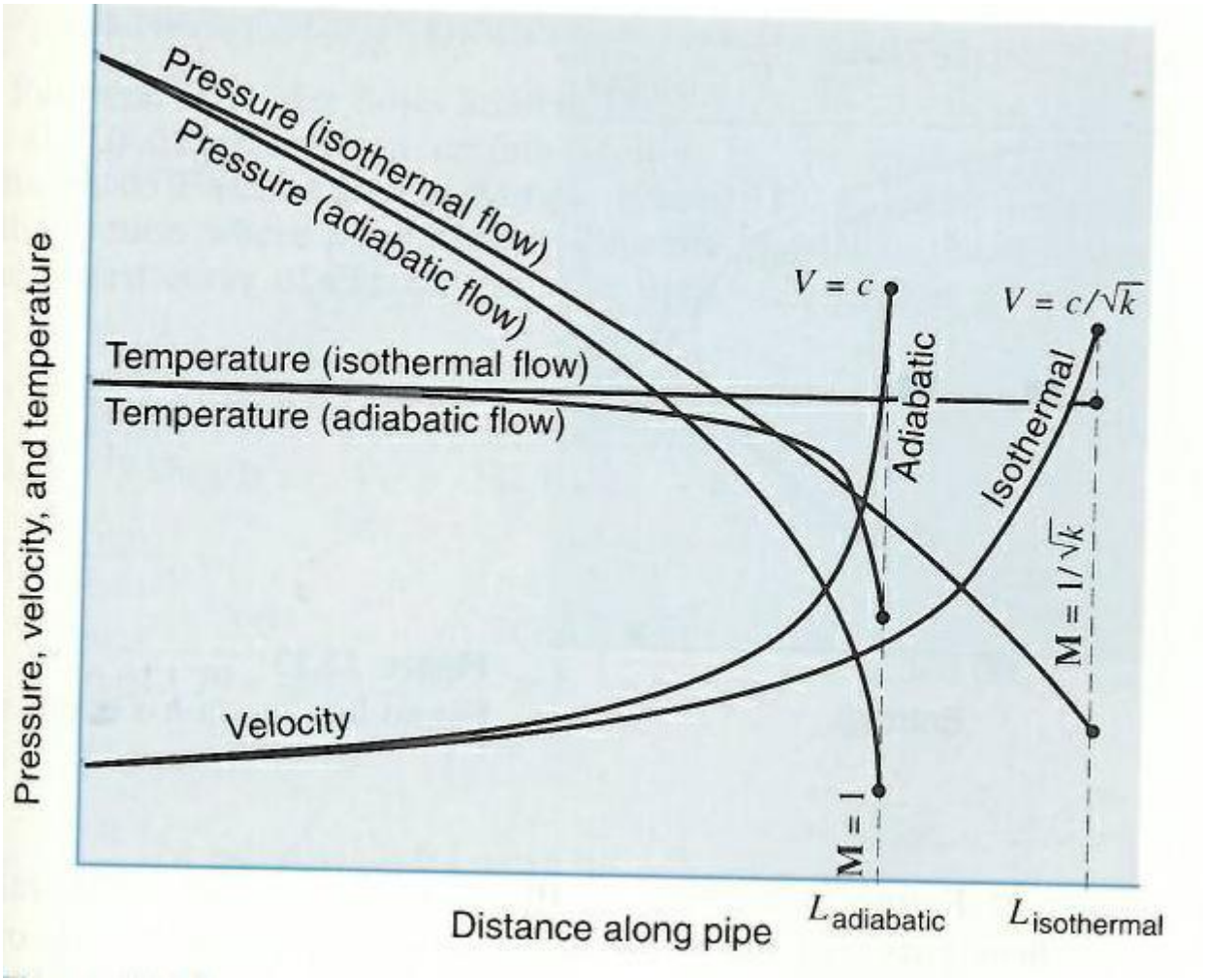

Isothermal and adiabatic flow compared at the same initial condition for air flowing in a pipe of constant diameter. [1]

Appendix D: Flare network piping information

24" Flare Stack - From KOD to Flare Tip

Pipe No	Length (m)	Elevation (m)	Material	ID (mm)	Wall thickness (mm)
1	15	2,5	Stainless Steel	609,6	14,27
2	18	3,0	Stainless Steel	609,6	14,27
3	25	25,0	Stainless Steel	609,6	14,27
4	25	25,0	Stainless Steel	609,6	14,27
5	30	30,0	Stainless Steel	609,6	14,27

30" Flare Header - From Flange to Flare KOD

Pipe No	Length (m)	Elevation (m)	Material	ID (mm)	Wall thickness (mm)
1	2	0	Carbon Steel	727,0	17,48
2	2	0	Carbon Steel	727,0	17,48
3	2	0	Carbon Steel	727,0	17,48
4	2	0	Carbon Steel	727,0	17,48
5	5	-2	Carbon Steel	727,0	17,48
6	8	-2	Carbon Steel	727,0	17,48
7	22	-3,7	Carbon Steel	727,0	17,48
8	14	-0,5	Carbon Steel	727,0	17,48
9	7	-0,2	Carbon Steel	727,0	17,48
10	9	-5,5	Carbon Steel	727,0	17,48
11	15	-0,5	Carbon Steel	727,0	17,48
12	41	-1,4	Carbon Steel	727,0	17,48

14" PSV Line - From PSV1 to Flare Header (Between pipe 1 & 2)

Pipe No	Length (m)	Elevation (m)	Material	ID (mm)	Wall thickness (mm)
1	0	0	Carbon Steel	152,4	10,31
2	3,5	-1,5	Carbon Steel	355,6	9,53
3	1,4	-1,4	Carbon Steel	355,6	9,53

14" PSV Line - From PSV2 to Flare Header (Between pipe 2 & 3)

Pipe No	Length (m)	Elevation (m)	Material	ID (mm)	Wall thickness (mm)
1	0	0	Carbon Steel	152,4	10,31
2	3,5	-1,5	Carbon Steel	355,6	9,53
3	1,4	-1,4	Carbon Steel	355,6	9,53

14" PSV Line - From PSV3 to Flare Header (Between pipe 3 & 4)

Pipe No	Length (m)	Elevation (m)	Material	ID (mm)	Wall thickness (mm)
1	0	0	Carbon Steel	152,4	10,31
2	3,5	-1,5	Carbon Steel	355,6	9,53
3	1,4	-1,4	Carbon Steel	355,6	9,53

Appendix E: Additional results tables

Nitrogen gas case:

	FlareNet				OLGA		
Position	Q, MSm3/D	Pressure, bar	Temparature, C	Mach	Pressure, bar	Temparature, C	Mach
upstream taipipe	2,5	1,471	19,480	0,245	1,602	39,400	0,184
	7,5	3,628	19,732	0,296	4,283	39,362	0,207
	15	7,212	22,022	0,297	8,571	40,147	0,206
	25	12,218	38,629	0,240	14,296	41,164	0,206
downstream tailpipe	2,5	1,460	19,431	0,247	1,516	39,025	0,195
	7,5	3,587	19,643	0,300	3,990	38,881	0,222
	15	7,131	21,899	0,301	7,984	39,637	0,221
	25	12,122	38,545	0,242	13,315	40,598	0,221
Upstream Flareheader	2,5	1,442	20,560	0,180	1,435	39,831	0,148
	7,5	3,522	21,226	0,220	3,710	39,993	0,171
	15	6,999	23,426	0,221	7,423	40,729	0,171
	25	11,963	40,197	0,177	12,378	41,637	0,171
Inlet KOD	2,5	1,382	21,811	0,009	1,389	38,480	0,007
	7,5	3,302	23,007	0,011	3,548	40,861	0,008
	15	6,563	25,058	0,011	7,101	42,071	0,008
	25	11,451	42,011	0,008	11,842	43,152	0,008
Upstream Flarestack	2,5	1,276	21,740	0,291	1,297	34,805	0,231
	7,5	2,878	22,750	0,386	3,224	35,841	0,279
	15	5,710	24,549	0,388	6,450	37,058	0,279
	25	10,514	41,811	0,287	10,753	38,101	0,279
Upstream Flare Tip	2,5	1,108	20,564	0,334	1,164	31,628	0,256
	7,5	2,062	17,017	0,531	2,716	32,517	0,329
	15	4,077	18,226	0,543	5,441	33,939	0,329
	25	9,075	39,806	0,331	9,074	34,998	0,329

Hydrocarbon gas case:

Case without 6-inch pipe between PSV and 14-inch tailpipe

	FlareNet					OLGA			
Position	Q, MSm3/D	Pressure, bar	Temparature, C	Ug, m/s	Mach	Q, MSm3/D	Pressure, bar	Temparature, C	Mach
Upstream tailpipe	2,5	1,2444497	20,16884343	80,24235999	0,197979967	2,5	1,36169	22,0273	0,182253
	7,5	2,508759158	19,13379612	118,4967676	0,292331026	7,5	3,04901	21,976999	0,243497
	15	4,926309403	20,57271017	120,3628813	0,296527829	15	6,06615	23,686701	0,24477
	25	8,180323941	22,64499057	120,4604911	0,297430531	25	10,0948	25,962099	0,244826
Downstream tailpipe	2,5	1,2384	20,14302365	80,62934983	0,198936201	2,5	1,29603	21,8234	0,191428
	7,5	2,4808	18,96852247	119,7761138	0,295505129	7,5	2,77446	21,333	0,267278
	15	4,8691	20,26505601	121,6770409	0,29973172	15	5,51451	22,8953	0,269116
	25	8,0852	22,29343674	121,7544111	0,300533088	25	9,17632	24,9785	0,269202
Upstream FH	2,5	1,2283	20,88897017	58,50128617	0,144270395	2,5	1,23638	22,386	0,144206
	7,5	2,4367	20,53945146	88,02028934	0,217081417	7,5	2,52186	22,228399	0,211527
	15	4,7796	21,85039642	89,49132272	0,220555048	15	5,00664	23,6392	0,213087
	25	7,9359	23,79742648	89,56855394	0,221253622	25	8,330410004	25,52339935	0,213280007
Inlet KOD	2,5	1,1957	21,6954789	2,755364967	0,006791049	2,5	1,20255	22,587	0,006782
	7,5	2,2879	22,30985227	4,314488418	0,010633151	7,5	2,35813	23,703899	0,010376
	15	4,4815	23,55495408	4,394197474	0,010829196	15	4,67903	25,1367	0,010458
	25	7,4434	25,38590884	4,397926514	0,010862851	25	7,78584	26,9266	0,010474
Upstream Flare Stack	2,5	1,1406	21,65520862	89,83204414	0,221398947	2,5	1,13391	20,4715	0,222853
	7,5	2,0060	22,13439112	153,0699082	0,377284188	7,5	2,04569	16,565399	0,367284
	15	3,9033	23,1908717	156,9739779	0,38678539	15	4,04983	17,750099	0,370881
	25	6,4776	24,81770959	157,300243	0,388179613	25	6,73697	19,4004	0,371276
Upstream Flare Tip	2,5	1,0596	21,29115719	96,63785725	0,238209601	2,5	1,03948	19,2523	0,242613
	7,5	1,4755	17,29587938	205,0534465	0,506691569	7,5	1,41638	10,2886	0,524203
	15	2,7952	17,27647781	215,5218049	0,531493688	15	2,77588	10,8707	0,533841
	25	4,6301	18,4070087	216,4325346	0,542607407	25	4,61742	12,0707	0,535058

Case with 6-inch pipe included between PSV and 14-inch tailpipe

	FlareNet					OLGA (CV=687000)		
Position	Q, MSm3/D	Pressure, bar	Temparature, C	Mach	Ug, m/s	Pressure, bar	Temparature, C	Mach
Upstream Tailpipe	2,5	1,4725	-5,801845569	0,87139055	335,7550712	2,4755	15,2789	0,537079
	5	2,9441	-4,61932224	0,87183634	335,2874801	4,63079	15,1298	0,572779
	7,5	4,4152	-3,474442469	0,87216237	334,7620941	6,87802	16,2953	0,578079
	10	5,8865	-2,318087373	0,87231947	334,2479461	9,15864	17,663099	0,578633
	12,5	7,3579	-1,169816676	0,87233515	333,7410928	11,4417	19,0322	0,578737
	15	8,8295	-0,030444264	0,87223667	333,2452444	13,7242	20,392099	0,578465
	17,5	10,3015	1,100413644	0,87203339	332,7606241	16,0047	21,7293	0,5783
	20	11,7738	2,221908068	0,87174577	332,291652	18,2838	23,0418	0,578026
	22,5	13,2467	3,333731489	0,87138057	331,8377769	20,56	24,33	0,577742
	25	14,7203	4,437066346	0,87093205	331,3947268	22,83	25,60	0,577468
Upstream Flareheader	2,5	1,2283	20,88897017	0,1442704	58,50128617	1,23799	24,9086	0,144696
	5	1,7491	20,40004612	0,20203228	81,88609893	1,79416	24,5203	0,199543
	7,5	2,4367	20,53945146	0,21708142	88,02028934	2,53203	24,755301	0,211678
	10	3,2018	20,92661893	0,21991342	89,21587246	3,35806	25,2115	0,212893
	12,5	3,9854	21,35608373	0,22057265	89,50585706	4,19329	25,684401	0,213115
	15	4,7796	21,85039642	0,22055505	89,49132272	5,02891	26,156799	0,213171
	17,5	5,5700	22,33444258	0,22070361	89,52097484	5,86505	26,6262	0,213317
	20	6,3567	22,81569901	0,22098871	89,58952546	6,7015	27,0965	0,213221
	22,5	7,1425	23,29890839	0,22122444	89,62593933	7,54	27,56	0,213412
	25	7,9359	23,79742648	0,22125362	89,56855394	8,37	28,02	0,213356
Inlet KOD	2,5	1,1957	21,6954789	0,00679105	2,755364967	1,2039	24,908199	0,006804
	5	1,6571	21,95967571	0,00979638	3,974288017	1,69253	25,6336	0,009691
	7,5	2,2879	22,30985227	0,01063315	4,314488418	2,36758	26,1688	0,010382
	10	3,0018	22,7126856	0,01079436	4,380827176	3,13822	26,6793	0,010444
	12,5	3,7381	23,12772421	0,01082565	4,393648917	3,91857	27,1628	0,010465
	15	4,4815	23,55495408	0,0108292	4,394197474	4,69998	27,6308	0,010462
	17,5	5,2182	24,01812701	0,01084753	4,399932963	5,4814	28,087601	0,01047
	20	5,9551	24,47460843	0,01086173	4,403371412	6,26381	28,5383	0,010467
	22,5	6,6977	24,92324822	0,01086405	4,401526803	7,04	28,98	0,010472
	25	7,4434	25,38590884	0,01086285	4,397926514	7,82	29,42	0,010477
Upstream Flarestack	2,5	1,1406	21,65520862	0,22139895	89,83204414	1,1348	22,759701	0,223683
	5	1,4881	21,85075142	0,33930213	137,6505704	1,49689	19,8248	0,337065
	7,5	2,0060	22,13439112	0,37728419	153,0699082	2,05368	18,973101	0,367595
	10	2,6181	22,47888555	0,38507177	156,2623698	2,7174	19,3402	0,369939
	12,5	3,2564	22,83396455	0,386633	156,917317	3,39192	19,7677	0,370732
	15	3,9033	23,1908717	0,38678539	156,9739779	4,0682	20,201799	0,371032
	17,5	4,5423	23,59040378	0,38761627	157,2802494	4,74416	20,6262	0,370989
	20	5,1816	24,01065761	0,38827134	157,4928674	5,42165	21,047199	0,371191
	22,5	5,8278	24,40338464	0,38831217	157,4382765	6,10	21,45	0,371351
	25	6,4776	24,81770959	0,38817961	157,300243	6,77	21,86	0,371434
Upstream Flare Tip	2,5	1,0596	21,29115719	0,2382096	96,63785725	1,0397	21,4079	0,243613
	5	1,1989	19,29347475	0,41857617	169,5694734	1,14779	15,9846	0,43657
	7,5	1,4755	17,29587938	0,50669157	205,0534465	1,4216	12,624	0,524746
	10	1,8808	16,8661978	0,52833582	213,8725145	1,8635	12,6187	0,533757
	12,5	2,3300	16,99401887	0,53209829	215,5729972	2,32611	12,9588	0,533708
	15	2,7952	17,27647781	0,53149369	215,5218049	2,78939	13,2906	0,533909
	17,5	3,2479	17,52742441	0,53289037	216,2556284	3,25362	13,6066	0,534288
	20	3,6994	17,77812049	0,54332029	216,8470139	3,71893	13,9206	0,534778
	22,5	4,1616	18,06964686	0,54329989	216,7590209	4,18	14,22	0,534908
	25	4,6301	18,4070087	0,54260741	216,4325346	4,64	14,51	0,535097

Appendix F: Nomenclature and Units

Symbol	Definition	Units
m	Mass	kg
ρ	Fluid density	kg/m^3
A	Cross-sectional area	m^2
$\dot{m}$	Mass flow rate	kg/h
p	Pressure	bara
T	Temperature	K
z	Compressibilty factor	-
R	Gas constant	m^3 bar K^{-1} mol^{-1}
υ	Volume	m^3
V	Control volume	m^3
s	Entropy	m^3 bar K^{-1} or J/K
h	Specific enthalpy	m^3 bar kg^{-1} or J/kg
c_v	Constant volume specific heat capacity	J/kg/K
c_p	Constant pressure specific heat capacity	J/kg/K
Q	Volumetric flow rate	m^3/s
U	Flow velocity	m/s
c	Speed of sound	m/s
g	Acceleration due to gravity	m/s^2
z	Elevation	m
M	Mach number	-
f	Fanning friction factor	-
L	Length	m
D	Inner diameter	m
γ	Specific heat ratio	-
U_{LS}	Superfacial liquid velocity	m/s
U_{GS}	Superfacial gas velocity	m/s
U_{mix}	Mixture velocity	m/s